Fakultät für Physik und Astronomie
Ruprecht-Karls-Universität Heidelberg

DIPLOMARBEIT

im Studiengang Physik

vorgelegt von

Elena Hassinger

aus Schwäbisch Hall

2007

Pressure-temperature phase diagram of URu_2Si_2 by ac-calorimetry and resistivity measurements

Die Diplomarbeit wurde ausgeführt von Elena Hassinger am

Kirchhoff-Institut für Physik

unter der Betreuung von

Herrn Prof. Dr. C. Enss

Untersuchung des Hochdruck-Phasendiagramms von URu_2Si_2 mittels AC-Kalorimetrie und Messung des spezifischen Widerstands

Zusammenfassung

Eines der interessantesten Themen im Gebiet der elektronisch hochkorrelierten Systeme ist die Konkurrenz verschiedener Grundzustände wie zum Beispiel Magnetismus und Supraleitung. Die sogenannten Schwere-Fermion Systeme sind aufgrund ihrer niedrigen charakteristischen Energie (Fermi-Temperatur) besonders zur Untersuchung einer solchen Konkurrenz geeignet, da der Grundzustand durch Druck oder ein Magnetfeld einfach verändert werden kann.

In dieser Arbeit wurde das Hochdruck-Phasendiagramm der Schwere-Fermion Verbindung URu_2Si_2 durch Messungen des spezifischen Widerstands und der spezifischen Wärme im Detail untersucht. Der hydrostatische Druck wurde von einer Diamant-Stempel-Druckzelle erzeugt und die spezifische Wärme mittels AC-Kalorimetrie gemessen. Alle Messungen wurden an derselben Probe durchgeführt. Bei Normaldruck werden in dieser Verbindung zwei aufeinander folgende Phasenübergänge beobachtet. Bei $T_0 = 17.5$ K geht das System in eine geordnete Phase über, deren Ordnungsparameter jedoch trotz intensiver Anstrengungen noch nicht eindeutig bestimmt werden konnte. In der Literatur wird diese Phase daher "versteckte Ordnung" genannt. In Neutronenstreuexperimenten wurde ein geordnetes magnetisches Moment von $m = 0.03\ \mu_B$ bestimmt; dieses ist allerdings viel zu gering, um die große Entropieänderung beim Phasenübergang zu erklären. Bei tiefen Temperaturen unterhalb von $T_{SC} = 1.4$ K wird die Verbindung zusätzlich supraleitend.

Unter Druck findet ein Übergang zu einer normalen antiferromagnetischen Phase mit einem größeren geordneten Moment statt. Das Zusammenspiel zwischen der versteckten Ordnung und der antiferromagnetisch geordneten Phase und deren Einfluss auf die Supraleitung wurde durch unsere Untersuchung besser verstanden: Das Phasendiagramm zeigt vier getrennte Bereiche. Die Grenzlinie zwischen der versteckten Ordnung und der antiferromagnetischen Phase konnte sowohl in den Messungen der spezifischen Wärme als auch des spezifischen Widerstands zum ersten Mal bestimmt werden. Sie steigt mit dem Druck steil an und trifft auf die Phasengrenzlinie $T_0(p)$. Die typische Form der Anomalie im spezifischen Widerstand beim Eintritt in die versteckte Ordnung, verursacht durch ein Umordnen der Fermi-Fläche unterhalb von T_0, wurde bis zum größten gemessenen Druck von $p = 5.5$ GPa beobachtet. Dies bedeutet, dass die mit der Umordnung einhergehende Spin-Dichte-Welle bis zu hohen Drücken fortbesteht und mit der antiferromagnetischen Phase koexistiert. Die Volumen-Supraleitung koexistiert mit der versteckten Ordnung, wird aber bei dem Druck unterdrückt, bei dem die antiferromagnetische Phase stabilisiert wird. Damit verhält sich URu_2Si_2 anders als übliche Schwere-Fermion Supraleiter auf Uranbasis, in denen eine mikroskopische Koexistenz von Supraleitung und Magnetismus beobachtet wurde.

Abstract

One of the most exciting topics in strongly correlated electron systems is the competition between different ground states like magnetic order and superconductivity. The so-called heavy fermion compounds are, due to their low characteristic energy (Fermi temperature), extremely suitable to study such a competition because the ground state properties can be modified easily by applying pressure or magnetic field.

In this work we have studied in detail the pressure-temperature phase diagram of the uranium based heavy fermion compound URu_2Si_2 by resistivity and ac-calorimetric measurements under highly hydrostatic pressure and at low temperature. All measurements were carried out on the same sample in a diamond anvil cell. At zero pressure this compound shows two successive phase transitions. The first transition occurs at $T_0 = 17.5$ K to the so-called "hidden order" phase. The nature of the order parameter of this phase is still unknown. The observed ordered magnetic moment of $m = 0.03\ \mu_B$ is too small to explain the enormous anomaly in specific heat, which is due to a condensation process where a gap opens on the Fermi surface. Below 1.4 K superconductivity coexists with this phase. Under pressure a probably first order transition to a usual antiferromagnetic phase with a larger ordered moment develops.

Our investigation sheds new light on the interplay between the different ground states. The pressure phase diagram we established shows four distinct regions. The transition line between hidden order and antiferromagnetism is seen in both resistivity and ac-specific heat for the first time. It shifts very strongly to higher temperatures with increasing pressure and joins the transition line $T_0(p)$. The typical shape of the resistivity, which is caused by the rearrangement of the Fermi surface, persists to the highest pressure we measured of $p = 5.5$ GPa, indicating that the spin density wave, associated to the rearrangement, is coexistent with the antiferromagnetic phase at high pressures. The superconducting phase is suppressed at the pressure where the antiferromagnetic phase emerges, whereas in other uranium based heavy fermion systems magnetism and superconductivity can microscopically coexist.

Contents

Introduction **1**

1 Theory **3**

1.1 Heavy fermion systems 3

1.2 Fermi-liquid theory 5

1.3 Kondo effect 6

1.4 RKKY interaction 8

1.5 Kondo versus RKKY interaction in heavy fermion compounds under pressure 8

1.6 Non-Fermi-liquid behaviour 11

1.7 Unconventional superconductivity 12

1.8 Spin density waves 13

2 URu_2Si_2 **15**

2.1 Ambient pressure results 16

2.2 URu_2Si_2 under pressure 22

3 Experimental methods **29**

3.1 Samples 29

3.1.1 Preparation and characterisation of the single crystals 29

3.2 Resistivity measurements 31

3.3 Ac-calorimetry under pressure 33

3.4 Pressure 35

3.4.1 Pressure cell 35

3.4.2 Gasket 36

3.4.3 Pressure transmitting element 37

3.4.4 Ruby method of pressure measurement 37

3.4.5 Changing pressure 38

3.4.6 In-situ pressure tuning 39

3.5 Cooling process 40
3.5.1 ^{3}He cryostat 40
3.5.2 ^{4}He cryostat 40
3.5.3 Dilution cryostat 41

4 Results **43**
4.1 Resistivity measurements 44
4.1.1 Transition between hidden order and antiferromagnetism. 46
4.1.2 Superconducting transition 47
4.2 Specific heat measurements 50
4.2.1 Superconducting transition 51
4.3 Discussion 53
4.3.1 Pressure-temperature phase diagram 53
4.3.2 Transition at T_0 57
4.3.3 Low temperature behaviour 61
4.3.4 Superconducting transition 62

Conclusion **65**

Introduction

URu_2Si_2 is member of a class of materials called heavy fermion compounds known for extraordinary low temperature properties. Especially since the discovery of unconventional superconductivity in some of these intermetallic compounds they have created much interest in the solid state physics community. Their particular properties, like an enormous specific heat or linear term of the resistivity at low temperature, cannot be described within the free electron model as in the simple metals copper or aluminium but they are rather an effect of strong interactions between the electrons. In theory the interactions are taken into account by introducing an effective mass, which can be up to 1000 times larger than the free electron mass. This is the reason why they are called heavy fermion systems, electrons being fermions. Moreover, they lie close to a quantum critical point, a transition point between two quantum phases. Under the action of an external parameter different from temperature (like pressure, magnetic field or chemical substitution) the ground state can be driven from a magnetic to a non-magnetic state. In proximity to such a phase transition, the systems are often superconducting, one can even find coexistence of magnetism and superconductivity.

In this Diplomarbeit we will focus on the unusual properties of the heavy fermion compound URu_2Si_2. At zero pressure this compound undergoes at 17.5 K a phase transition to an ordered state. Despite considerable experimental and theoretical efforts for more than 20 years, the order parameter is not yet totally understood and therefore the phase is called "hidden order". At low temperature a superconducting state coexists with this phase with $T_{SC} \approx 1.4$ K.

In the present study pressure is used as a tool to tune the strength of interaction between the electrons. The pressure-temperature phase diagram of URu_2Si_2 is particularly rich. At low pressures up to ~ 0.5 GPa the hidden order phase is predominant and at higher pressures a usual antiferromagnetic phase develops. At the same time, superconductivity is suppressed. The behaviour of the phase transitions under pressure and especially the interplay and competition of the hidden order and the antiferromagnetic phase will be investigated and a detailed pressure phase diagram will be established in order to understand the phases at ambient pressure.

The experimental techniques used for this study are ac-calorimetry and resistivity measurements under high pressure and at low temperature. The specific heat gives us information about the entropy of the system, especially entropy changes at phase tran-

sitions. Resistivity measurements allow a view on the scattering of conduction electrons and are sensitive to changes at the Fermi surface. Pressures up to 5.5 GPa are generated in a diamond anvil cell. This guarantees highly hydrostatic pressure conditions, but entails sample sizes smaller than half a millimeter. Under these conditions the experimental realisation is not easy and demands developed fine motor skills. Low temperatures down to 60 mK are attained with standard cryostats.

In the following work I will first explain the most important aspects of theory which are necessary to understand heavy fermion systems in general and especially the compound URu_2Si_2. In the second chapter I will introduce previous results of URu_2Si_2 at ambient pressure and under high pressure published before the beginning of my Diplomarbeit. The third chapter will then treat the experimental technique of resistivity and ac-calorimetry measurements under pressure and at low temperature before we present our results in the last chapter and discuss them regarding also the latest publications of other groups.

Chapter 1

Theory

URu_2Si_2 is a uranium based heavy fermion system. It undergoes two succesive phase transitions: one at ~ 17.5 K to hidden order and the transition to superconductivity at ~ 1.4 K. This chapter first gives an overview of the important physical phenomena in heavy fermion compounds before describing subsequently the physical effects, interactions and theoretical models in question more in detail. The last paragraph deals with an antiferromagnetic ground state which could possibly be a candidate for the hidden order state.

1.1 Heavy fermion systems

Heavy fermion compounds are intermetallic compounds which contain rare earth elements like cerium (Ce) or ytterbium (Yb) or actinides like uranium (U). Famous representatives are for example $CeAl_3$ or $CeCu_2Si_2$ [1]. These elements have a partly filled $4f$-shell for ytterbium and cerium and $5f$-shell for uranium. The $4f$-states are well localised (see figure 1.1b) in real space, that means close to the atomic core compared to the closed $5s$ and $5p$-shells because of the strong centrifugal potential $l(l+1)/r^2$ with l=3 for f-electrons. Therefore they keep their atomic like character even in solids. Nevertheless the tail of their wave function at the outside of the closed $5s$ and $5p$-shell is not negligible. This part of the wave function can easily be influenced by the potential energy, crystal field and the distance between the lanthanide atoms and it overlaps with the conduction electron wave function. In energy space the $4f$-level is narrow and lies near the Fermi energy so that the corresponding electrons can interact and hybridise with the conduction electrons. This evokes spin- and valence fluctuations.

The low temperature behaviour of macroscopic properties in heavy fermion systems can first be analyzed by Landau's Fermi-liquid theory [2]. In this theory strongly interacting fermions are substituted by weakly interacting quasiparticles with an enhanced effective mass, which results in very large specific heat, susceptibility and resistivity at low temperature. The most important results of this theory are given in paragraph 1.2.

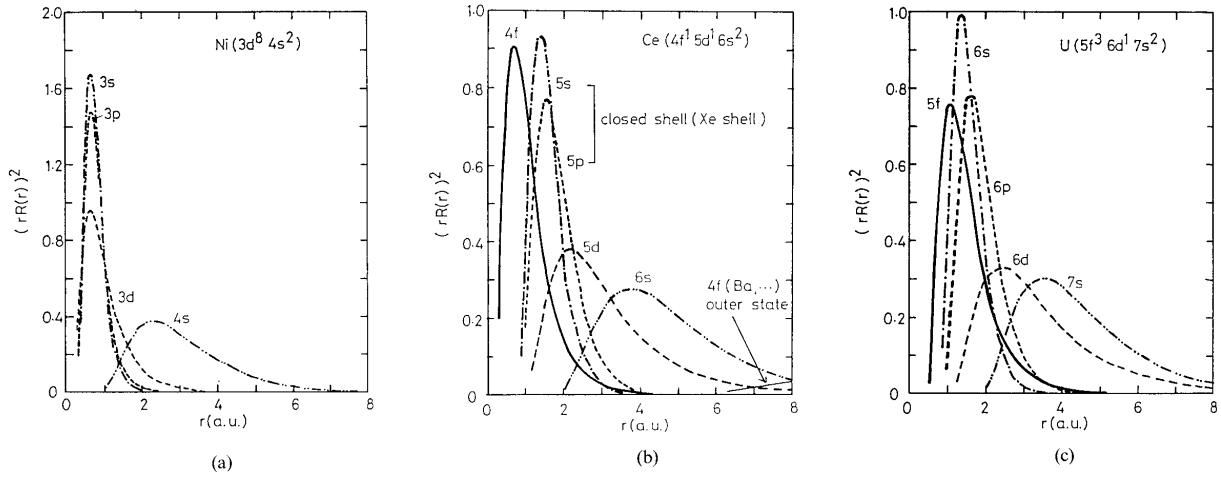

Fig. 1.1 : Effective radial charge densities of (a) Ni, (b) Ce and (c) U atoms [4].

At high temperature these systems show a Curie-Weiss like behaviour of the susceptibility $\chi \propto \frac{\mu_{eff}^2}{T-\Theta}$ due to the weakly interacting magnetic moments of the $4f$ respectively $5f$-electrons. Curie-Weiss temperature Θ_{CW} is often smaller than zero and the effective magnetic moment μ_{eff} usually larger than 2 μ_B. However, it usually does not exactly correspond to the value calculated by Hund's rules for the electron configuration of the free ion because of the crystal field splitting.

At lower temperatures the local moments are screened by the spins of the conduction electrons like in metals with dilute magnetic impurities. We will introduce the Kondo effect shortly in paragraph 1.3. Additionally the local moments interact indirectly via the conduction electrons by the RKKY interaction (see paragraph 1.4 [3]). The competition between the RKKY interaction which favours long range magnetic order and the moment screening of Kondo effect leads to different ground states in heavy fermion systems (see paragraph 1.5). At zero temperature the system can be driven from a magnetically ordered ground state to an non-magnetic state by changing a parameter other than temperature. This parameter, notably pressure, magnetic field or chemical substitution tunes the strength of the two competing forces. Such a phase transition happens at a quantum critical point. In the vicinity of this point usually the typical properties of a Fermi liquid are violated at least down to a rather low temperature and so-called Non-Fermi-liquid behaviour is found (see paragraph 1.6).

In uranium the $5f$-states are less localised as shown in figure 1.1c) where you can see the effective radial charge density of the U atom compared to those of Ce and Nickel (Ni) 1.1b and a), the latter being a typical magnetic system with itinerant (delocalised) $3d$-electrons. We see that the f-state in uranium has a more itinerant character than in Ce and the $5f$-wave function is between atomic-like (as in Ce) and band-like (as the $3d$-state in Ni). As a consequence, magnetism in U compounds probably also has a more

itinerant character. In the dual modal which is applicable for example for UPd_2Al_3, one of the three $5f$-electrons is delocalised and the two other ones are localised [5]. In general, uranium compounds with strong electronic correlations show a high complexity. Not only the unknown degree of itineracy but also the presence of several competing energy scales such as strong magnetic anisotropies, strongly hybridised crystal field excitations and soft lattice modes play a role.

There are some heavy fermion systems which show unconventional superconductivity (see paragraph 1.7), for example $CeCu_2Si_2$, UPt_3, URu_2Si_2 or UPd_2Al_3. Highly interesting phenomena like coexistence of superconductivity with magnetic ordering, anisotropic gaps and coupling of cooper pairs by magnetic or valence fluctuations need further investigation.

1.2 Fermi-liquid theory

Electrons in a solid interact by Coulomb interaction. In heavy fermion systems, the interaction cannot be neglected like for example in the normal metal copper. In the Fermi-liquid theory the interacting electrons are described as weakly interacting quasiparticles. Concerning their motion the interaction is taken into account by introducing an effective mass m^* in terms of Landau parameters [2]. The quasiparticles are excitations of this N body system where the only difference to the excited states of free electrons is the renormalized effective mass. A simple image would be that, when an electric field is applied, the electrons cannot move easily or freely like in an electron gas because of their interaction with the other electrons which gives them a larger inertia and so a larger mass. In this theory the low temperature properties follow the following laws: The specific heat C divided by temperature is given as:

$$\frac{C}{T} = \gamma + \beta T^2 \tag{1.1}$$

The second term is the phonon contribution and the first term originates from the quasiparticles. γ is called the Sommerfeld coefficient and given as

$$\gamma = \frac{\pi^3}{3} k_B^2 N(E_F) = \frac{k_F k_B^2}{3\hbar^2} m^*. \tag{1.2}$$

Here, k_F is the radius of the Fermi sphere, k_B is the Boltzmann constant and $\hbar$ Planck's constant.

The susceptibility χ is calculated as

$$\chi = \chi_0(1 - aT^2) \tag{1.3}$$

with

$$\chi_0 = \mu_0 \mu_B^2 N(E_F) \propto n^{1/3} m^* \tag{1.4}$$

In first order this is a Pauli susceptibility proportional to m^*. In case of magnetic interactions, for example ferromagnetic interactions, there may be another factor of enhancement introduced by another Landau parameter G_0.

For $T \longrightarrow 0$ the susceptibility and the specific heat depend both on the density of states on the Fermi surface $N(E_F)$. The so called Wilson ratio

$$R = \frac{\chi}{\gamma} \frac{\pi^2 k_B^2}{\mu_0 \mu_{eff}^2} \tag{1.5}$$

is one for free electrons but between two and five for heavy fermion systems. The enhancement is due to the additional Landau parameter G_0 in the susceptibility.

For the resistivity in Fermi-liquid theory we obtain:

$$\rho = \rho_0 + AT^2. \tag{1.6}$$

with $A \propto m^{*2}$. The first term is due to scattering at impurities and defects and the second term is due to quasiparticle quasiparticle scattering. This crude proportionality of χ, C/T and A to m^* and m^{*2} is roughly valid since in heavy fermions the spin dynamics and the mass enhancement is dominated by local fluctuations. By contrast in $3d$ itinerant magnetism where the phenomena occur around a given wavevector this proportionality is not observed.

1.3 Kondo effect

The signature of the Kondo effect is a minimum in resistivity of metals with dilute magnetic impurities, that means that the resistivity rises again when lowering the temperature (see figure 1.3). This behaviour has first been explained by Kondo [6] who introduced the perturbation term

$$H_K = -2J \, \boldsymbol{S} \cdot \boldsymbol{s} \tag{1.7}$$

into his Hamiltonian. It describes the scattering of conduction electrons with spin $\boldsymbol{s}$ with a local moment $\boldsymbol{S}$ of the impurity. J is the exchange integral of the attributed spin wave functions. The interaction is antiferromagnetic and owing to higher order processes the spins of the conduction electrons form a screening cloud around the local moment. At low temperature the hybridisation V of conduction electrons with the d or f-electrons responsible for the local moment $\boldsymbol{S}$ leads to a peak in the density of states at the Fermi level called Kondo resonance or Abrikosov-Suhl resonance (see figure 1.2). This peak develops to compensate the loss of degrees of freedom of the spin and the orbital moment of the conduction electrons. Its width is $\sim k_B T_K$. It is this large density of states which leads to the enhanced effective mass in heavy fermion compounds.

A simple image would be that in the ground state the spin $\boldsymbol{S}(\uparrow)$ and the spin $\boldsymbol{s}(\downarrow)$ form a non-magnetic bound singlet state $\{\boldsymbol{S}(\uparrow) \cdot \boldsymbol{s}(\downarrow) \pm \boldsymbol{S}(\downarrow) \cdot \boldsymbol{s}(\uparrow)\}$ with a binding

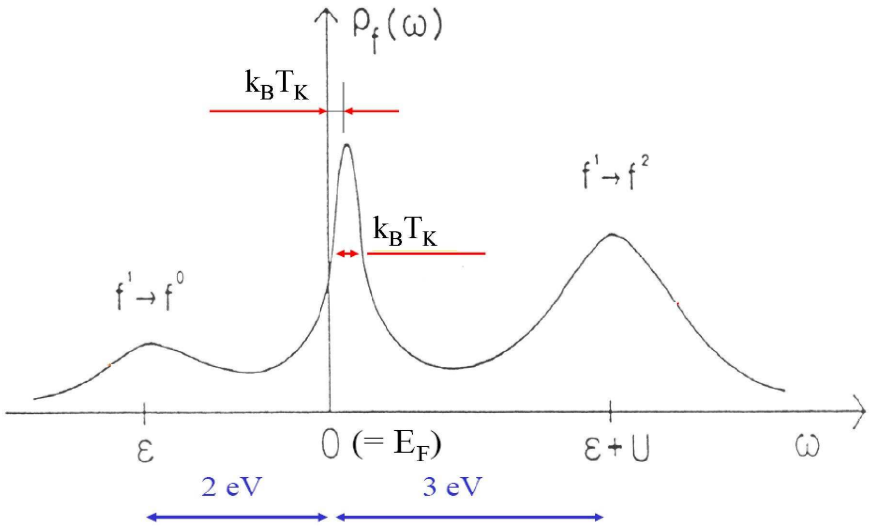

Fig. 1.2 : In the Kondo model a maximum (Kondo resonance) develops in the density of states near the Fermi energy due to hybridisation. The virtual $4f$-level has a distance of $\epsilon \approx 2$ eV from the Fermi level. The Coulomb repulsion against one electron more in the $4f$-level is ~ 5 eV [7].

energy

$$k_B T_K \propto D \exp(-\frac{1}{N(E_F)J}) \tag{1.8}$$

$N(E_F)$ is the number of charge carriers at the Fermi surface and D is linked to the width of the virtual bound state of the magnetic impurity.

Just above the Kondo-temperature T_K the resistivity of a metal with magnetic impurities rises when lowering the temperature (see figure 1.3) according to the following equation

$$\rho \propto -ln(\frac{T}{T_K}) \tag{1.9}$$

Remarkably in heavy fermion systems, where the magnetic "impurities" i.e. the moments of the f-electrons, are present on every cerium-lattice site, the Ce f-electrons behave just above the Kondo-temperature like diluted magnetic moments in spite of their periodicity. Only at a still lower temperature T_{coh} coherence effects start to play a role and the correlations between impurity spins and spins of conduction electrons become important on an extended length scale. Below this temperature Bloch-waves develop and a band of quasiparticles is formed. In these Kondo lattices the resistivity drops strongly due to coherent scattering and follows at low temperature a Fermi-liquid behaviour (dashed line).

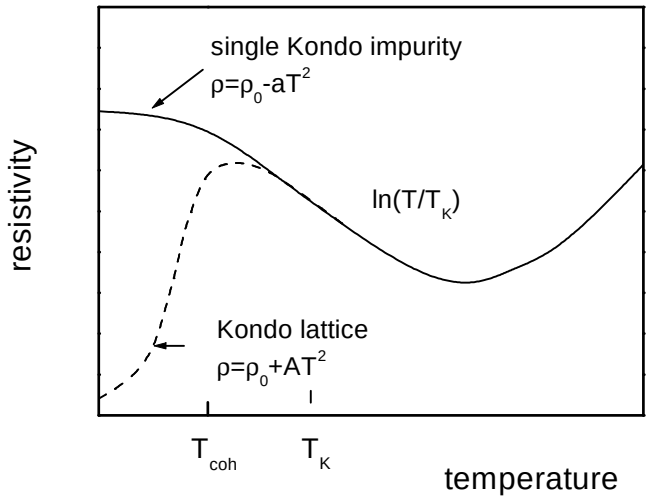

Fig. 1.3 : Temperature dependence of resistivity of a metal with the Kondo effect.

1.4 RKKY interaction

The wave functions of f-electrons are well localised and therefore the corresponding moments cannot interact directly with each other. But the spin polarised screening cloud of conduction electrons described in the paragraph about the Kondo effect (see paragraph 1.3) has a longer range and can mediate indirectly an interaction between two local moments. This so-called Rudermann, Kittel, Kasuya, Yosida (RKKY) interaction extends over a long range and damps with a sinusoidal oscillation with a wave vector k_F [3]. Depending on the distance between the magnetic moments $\boldsymbol{S_i}$ and $\boldsymbol{S_j}$ it can be ferro- or antiferromagnetic. The associated energy is:

$$k_B T_{RKKY} = J^2 N(E_F) \frac{\cos(k_F r)}{(k_F r)^3} \tag{1.10}$$

1.5 Kondo versus RKKY interaction in heavy fermion compounds under pressure

Kondo interaction and RKKY interaction both depend on the exchange J between the conduction electrons and the f-electrons. The system will take the ground state with the lower energy, that means where the energy gain is higher. If the RKKY interaction is stronger, this will be a magnetic ground state but if the Kondo interaction is stronger it will be a non-magnetic one. The competition of those two interactions has been studied by Doniach [8]. In the Doniach diagram (see figure 1.4) he draws the energies attributed to these two interactions as function of $JN(E_F)$. Heavy fermion systems are systems with a value of $JN(E_F)$ for which the associated energies $k_B T_K$ and $k_B T_{RKKY}$ have a similar value. By varying J, the system can be tuned from a magnetic to a non-magnetic system

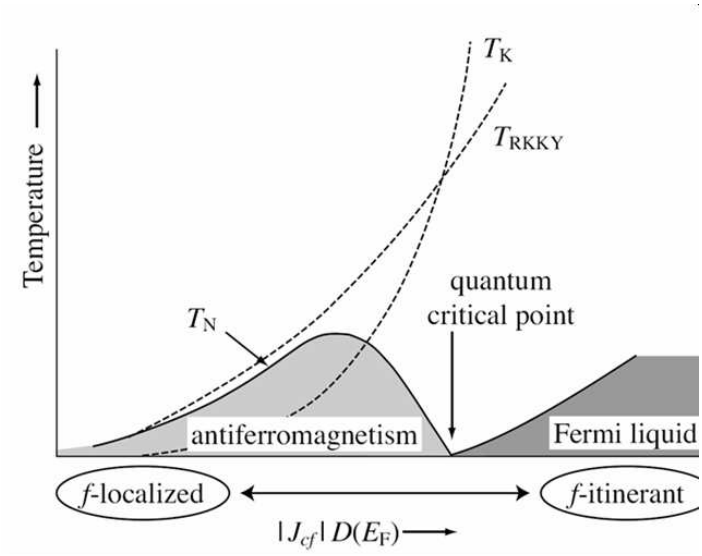

Fig. 1.4 : The Doniach phase diagram shows the competition between the energies associated to the Kondo effect T_K and the RKKY interaction T_{RKKY} as a function of $JD(E_F)$ (corresponds to $JN(E_F)$ in the text) and the corresponding ordering temperature T_N [9].

by passing a quantum critical point. This is a transition point at zero temperature where the ground state of the system passes from one quantum state to another driven by an external parameter other than temperature.

A possible parameter to tune the system through a quantum critical point is pressure. When pressure is applied, obviously the lattice parameters change and also the exchange integral between the conduction electron and the f-electron wave function. In energy space schematically presented in figure 1.5 the width of the virtual $4f$ bound state is defined as 2Δ and its distance to the Fermi level E_F is ϵ_{4f} where we find the Kondo resonance. In case of a strong Coulomb repulsion within the f-orbital (U$\longrightarrow \infty$) the exchange J, the hybridisation matrix element V and the width Δ fulfil the relations [10]:

$$JN(E_F) \approx \frac{\Delta}{\epsilon_{4f}} \qquad \Rightarrow \qquad J = \frac{V^2}{\epsilon_{4f}} \tag{1.11}$$

as $\Delta = V^2\mathrm{N(E}_F)$. Under pressure the f-level becomes wider and its energy level can also change. With a larger Δ and smaller ϵ_{4f} (in case of Ce) also the hybridisation and the exchange increase. This tunes the two competing forces and we move on the Doniach diagram.

Uranium as a free neutral atom has the electron configuration $[\mathrm{Rn}]5\mathrm{f}^3 6\mathrm{d}^1 7\mathrm{s}^2$. In a solid the most usual ions are U^{3+} with the configuration $[\mathrm{Rn}]5\mathrm{f}^3$ or U^{4+} with the configuration $[\mathrm{Rn}]5\mathrm{f}^2$. Both of these states are magnetic but the magnetic moments calculated by Hund's rules are never found in uranium compounds, because of the delocalisation of some of the $5f$-electrons. The delocalised f-electrons form bands and cannot contribute to the

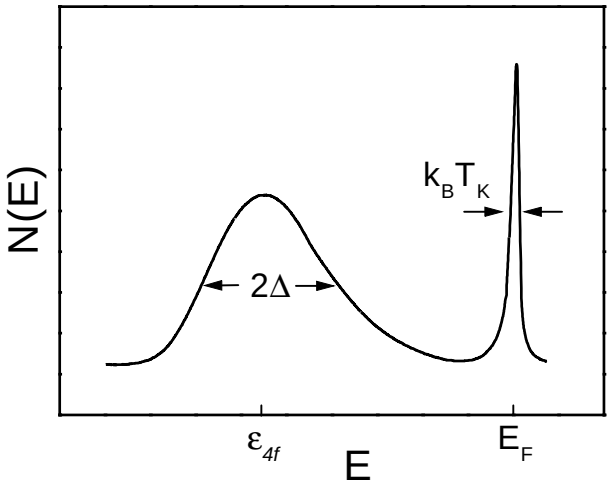

Fig. 1.5 : Schematic density of states of a heavy fermion system. The $4f$-level with a width 2Δ is localised with a distance of ϵ_{4f} from the Fermi energy E_F.

stable local moment. Under pressure the hybridisation increases and the f-electrons tend to escape into the conduction band and therefore the occupation of the f-level decreases.

The comportment of uranium can qualitatively be described [11] in a model of f-electron systems in a crystal where core electrons of an atom are localised in spheres around the nucleus with a diameter equal to the lattice parameter. The spheres of neighbours touch. i) When pressure is applied, the atomic distance is reduced and consequently the core region becomes also smaller. As a result, the core electrons screen the core potential more effectively so that it decreases. It is then less attractive for the f-electrons whose orbitals spread out more of their waves outside the core region in real space. Being large the latter are distorted by the crystal field and loose their f-character. Thus in a crystal there will never be 14 available f-states and the occupancy of the available f-states diminishes with pressure or from system to system with decreasing atomic distance. ii) The diffusion of the f-wavefunctions causes a higher overlap with the conduction band which results in a larger hybridisation. As a consequence, the hybridisation-induced two-ion coupling (RKKY) also grows with pressure. iii) In the density of states pressure leads to a broadening of the f-level, an f-band can be formed and f-electrons can hop from site to site. This is the reason why not all f-electrons contribute to the stable local moment. So by applying pressure (i) f-waves are turned into non-f-waves due to spectral loss in real space and (iii) localised f-waves are turned into itinerant f-waves due to spectral loss in energy space. These effects weaken the magnetic ordering and compete with the strengthened two-ion coupling(ii).

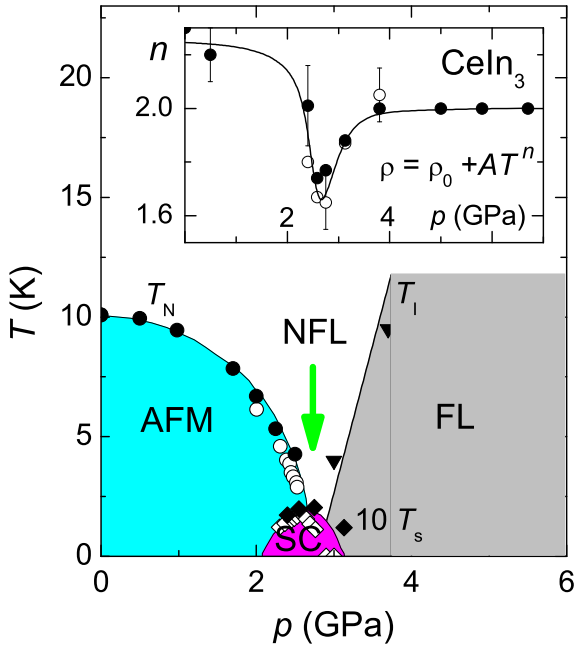

Fig. 1.6 : Pressure-temperature phase diagram around a quantum critical point for $CeIn_3$. The inlay shows the pressure dependence of the exponent n of a $\rho = \rho_0 + AT^n$ fit. [12]

1.6 Non-Fermi-liquid behaviour

In proximity to a quantum critical phase transition heavy fermion systems often exhibit strong deviations from Fermi-liquid theory due to strong spin fluctuations or valence fluctuations [13, 14]. As a typical example we present the pressure-phase diagram around a quantum critical point for $CeIn_3$ in figure 1.6. For low pressure $p < p_c$ the system is magnetically ordered. Coming close to the quantum critical point at p_c the spin fluctuations become stronger and stronger and the associated energy T_{sf} becomes larger. If the transition is of second order the spin correlation length ξ_s diverges at the quantum critical point. The characteristic spin fluctuation time τ_s is related to ξ_s via the critical exponent z as $\tau_s \sim \xi_s^{-z}$. At the quantum critical point the temperature T_N is so low that the magnetic order cannot be established down to zero temperature. In this fluctuation dominated region non-Fermi-liquid behaviour is found. For two and three dimensional spin fluctuations in a ferro- (F) or antiferromagnet (AF) the temperature dependence of resistivity ρ and specific heat C/T is given in tabular 1.6. The exponent n of the temperature behaviour of resistivity $\rho = \rho_0 + AT^n$ as a function of pressure for $CeIn_3$ is shown in the inlay of figure 1.6. It is smaller than two near the quantum critical point but equal to two for higher pressures. On this side of the quantum critical point the system recovers a Fermi-liquid behaviour.

		C/T	$\rho \sim T^n$
F	3d	$-lnT$	$T^{\frac{5}{3}}$
	2d	$T^{-\frac{1}{3}}$	$T^{\frac{4}{3}}$
AF	3d	$T^{\frac{1}{2}}$	$T^{\frac{3}{2}}$
	2d	$-lnT$	T

Table 1.1: Temperature variation of C/T and ρ in the non-Fermi-liquid regime [10].

1.7 Unconventional superconductivity

Heavy fermion superconductivity appears usually at a transition temperature $T_{SC} \leq 2$ K. Below this temperature the heavy quasiparticles condense into cooper pairs. The fact that quasiparticles and not light electrons take part in the condensation process can be seen from the size of the jump in specific heat $\Delta C \sim \gamma T_{SC}$ which is large due to the enhanced effective mass $\gamma \propto m^*$. Another surprising feature is that the superconductivity occurs even in presence of magnetic ordering or near a quantum critical point. In classical BCS theory with s-wave pairing magnetic impurities destroy superconductivity because the cooper pair electrons have opposed spin and propagation vector k. In magnetic materials however it is possible to find cooper pairs with total spin S = 1, 3... i.e. the cooper pair wave function is not an s-wave but a p- or d-wave. In heavy fermion systems superconductivity is often found in proximity of a quantum phase transition [15]. Therefore one might suspect, that it is the magnetic fluctuations which mediate the attraction between the members of a cooper pair and not phonons as in BCS theory. Unconventional superconductivity is characterized by a gap showing not the full lattice symmetry. For both conventional and unconventional superconductivity the order parameter can vanish on lines or points on the Fermi surface but in unconventional superconductivity the order parameter changes its sign at these points. In these special directions there is no gap and as a consequence no exponential temperature dependence of physical properties below the transition but simple power laws. The slope of the critical field $\mu_0 H_{c_2}$ (the external magnetic-field where superconductivity is suppressed by field and temperature) for $T \longrightarrow T_{SC}$ is given as

$$\left.\frac{\partial \mu_0 H_{c_2}}{\partial T}\right|_{T=T_{SC}} \propto m^{*2} T_{SC} \tag{1.12}$$

The value and temperature dependence of the critical field $\mu_0 H_{c_2}$ are determined from basically two mechanisms:

- Orbital pair breaking: the cooper electrons move in a magnetic field and are exposed to the Lorentz force which tends to separate the pair. As a result, the transition temperature is decreased. This is the limiting mechanism near T_{SC}.

- Pauli limiting: In a conventional singlet BCS superconductor the spins of the cooper

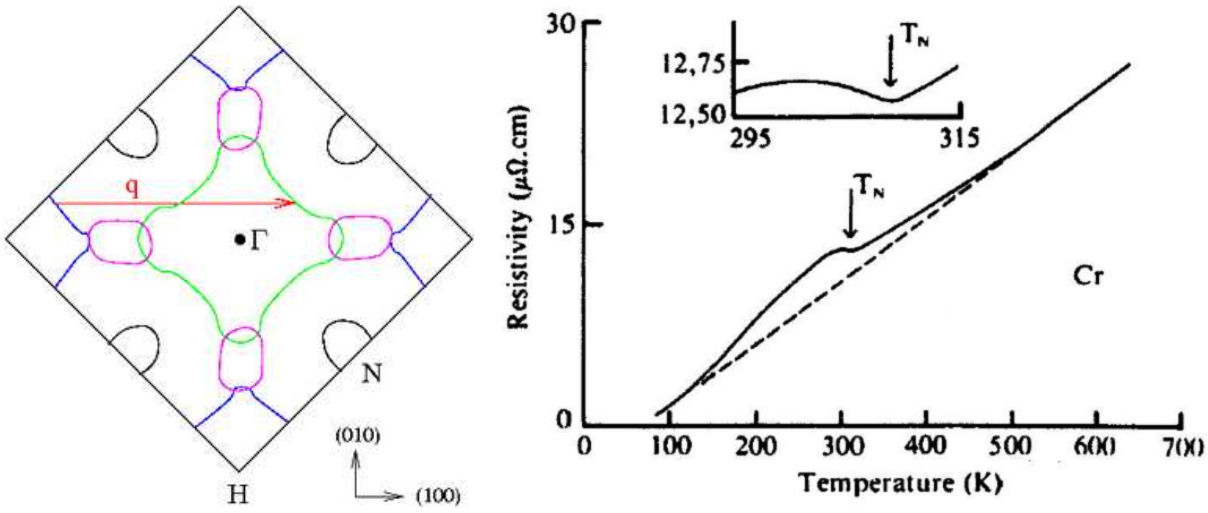

Fig. 1.7 : Left side: A sketch in k-space of a (0, 0, 1) section of the Fermi surface of Cr. The band structure of Cr yields an electron pocket (green) centred at Γ and a hole pocket (blue) centred at H. The surrounding black square represents the first Brillouin zone boundary. Right side: The typical nesting shape in the resistivity of chromium. [16]

electrons are opposed. Applying a magnetic field tends to align them and will in this way break the pair. This also reduces the transition temperature in field. It is of course not present in simple triplet states with S=1 and L=1, 3, ...

1.8 Spin density waves

The spin density wave state is an itinerant antiferromagnetic ground state. It often occurs in low dimensional or highly anisotropic systems. The most famous representative of systems with this ground state is chromium (Cr) [17, 18]. On the left side of figure 1.7 is sketched the Fermi surface of chromium in k-space perpendicular to the (0, 0, 1) direction. The band structure of Cr shows an electron pocket (green) centred at Γ and a hole pocket (blue) centered at H. The boundaries of these two kinds of pockets have large parallel regions that match when shifted by the nesting wavevector q (red). If this nesting is possible, the electrons and holes condensate into the spin density wave state with a sinusoidal or helical variation of the spin density. The charge density meanwhile stays constant implying an opposite variation of the density of fermions with spin up and spin down. The energy gain for the condensate is $\Delta N(E)$ with the gap Δ which opens on the concerned part of the Fermi surface. The gap opening leads to a loss of carrier density and therefore firstly to an increase in the resistivity curve below the Neel temperature T_N (see figure 1.7 on the right) and secondly to a BCS like exponential decay in resistivity and specific heat. If q is a rational multiple of the lattice constant a, the spin density wave is said to be commensurate, otherwise it is incommensurate. The real space periodicity of the resulting spin density wave is given by 2π/q. The spin

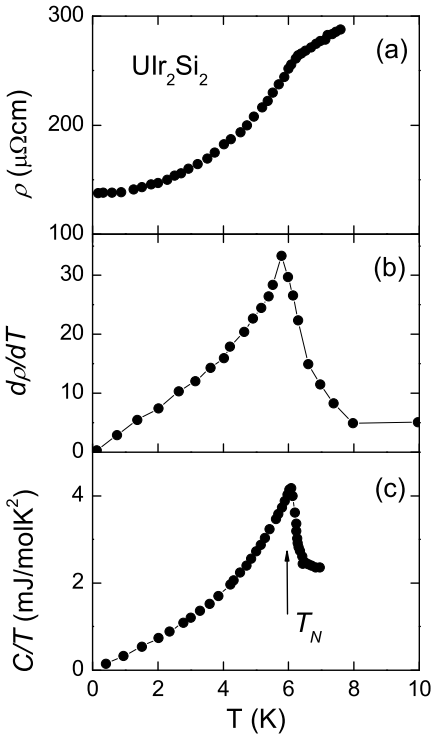

Fig. 1.8 : Temperature dependence of resistivity (a), derivative of resistivity (b) and specific heat (c) of UIr_2Si_2 [19, 20]. Lines are guides to the eye.

density wave state is an antiferromagnetic ground state. The typical nesting signature of the resistivity at the phase transition is different from the signature of a transition to "normal" antiferromagnetism. As and example for the signature of an antiferromagnetic transition without nesting, we present in figure 1.8 data for UIr_2Si_2, another example out of the same class of compounds with UT_2Si_2 structure (T is a transition metal). Here the resistivity just makes a downward kink at T_N and its derivative is similar to the specific heat.

Chapter 2

URu_2Si_2

In 1985 during systematic studies of CeT_2Si_2 and UT_2Si_2 compounds, where T is a transition metal, interest fell on URu_2Si_2. It is a heavy fermion compound with a slightly enhanced mass. Two successive phase transitions were seen as large anomalies in macroscopic properties like specific heat and susceptibility [21], one at $T_0 \approx 17.5$ K and the other one at $T_{SC} \approx 1.4$ K to unconventional superconductivity. Below T_0 an antiferromagnetically ordered phase (AF) with a very small ordered moment of $m \approx 0.3\ \mu_B$ is found [22], which cannot account for the large loss of entropy $\Delta S \approx 0.2R \ln 2$ at T_0. The order parameter accountable for this symmetry change is still not known and therefore the phase is called "Hidden Order" phase.

Neutron scattering measurements under pressure revealed a new antiferromagnetic phase with a large ordered moment (LMAF) coming up for pressures larger than a critical pressure p_{c1} [23, 24]. However nuclear magnetic resonance (NMR) [66] and muon spin resonance (μSR) [25] measurements showed that not the ordered magnetic moment but the volume fraction of the magnetically ordered phase is small at ambient pressure and increases under pressure. Additionally the critical pressure depends quite strongly on the sample [24] and this phase transition is extremely sensitive to uni-axial stress in some crystallic directions [26]. This points towards the interpretation that at ambient pressure a small volume fraction of the sample is antiferromagnetic due to inner strains caused by defects but that the hidden order phase itself is nonmagnetic. Nevertheless some arguements suggest that the ordered moment is intrinsic to hidden order for example the fact that the order temperature of the small moments is also T_0. Under pressure T_0 increases first slowly until $p_{c2} \approx 1.4$ GPa and then faster in the large moment antiferromagnetic phase [27]. Although basic differences between the hidden order phase and the antiferromagnetic phase are expected, the signature of the transition in macroscopic measurements as far as it has been studied is quite similar for low and high pressures [28]. Here much more detailed studies are necessary looking at the signature of the transition with different macroscopic measurement techniques.

First neutron scattering measurements showed that the small ordered moment was

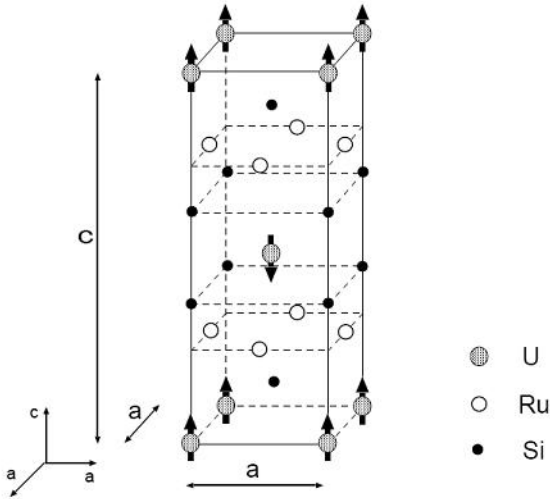

Fig. 2.1 : Crystal structure of URu_2Si_2 with ordered moments of the uranium atoms below $T_N = 17.5$ K.

even present in the superconducting phase, hence the compound was believed to be a candidate for coexistence between antiferromagnetism (AF) and superconductivity (SC) [22]. In resistivity measurements the superconducting transition is visible up to pressures far into the AF regime [27, 29]. Newer ac-susceptibility results claim that bulk superconductivity is suppressed under pressure by the AF phase [30]. In case of volume separation, this might mean that superconductivity would be only coexistent with the hidden order phase and not with magnetism.

Finally several open questions are left. Their answer could provide clues to the nature of the hidden order parameter: Is superconductivity coexistent with antiferromagnetism? What is the interplay between the order parameters in hidden order and antiferromagnetism? Are they coexisting or not? Is the low moment antiferromagnetism intrinsic to hidden order? How do the transitions change under pressure? Important for the symmetry of the order parameters is also, if the first order transition line in the pressure-temperature phase diagram has a critical endpoint or if we find two separated regions.

2.1 Ambient pressure results

URu_2Si_2 is a uranium based heavy fermion system. It has the body centred tetragonal $ThCr_2Si_2$ crystal structure with I4/mmm group symmetry (see figure 2.1)[21]. Its lattice parameters are a = b = 4.124 Å, c = 9.5817 Å at 4.2 K. These values are $\sim$ 0.1 % smaller than the values at room temperature hence the crystal structure does not change upon cooling [21]. After Schlabitz *et al.* had found hints to superconductivity in polycrystalline samples of URu_2Si_2, single crystals have first been studied by Palstra *et al.* in 1985 [31, 21]. They measured the specific heat (of an annealed polycrystalline sam-

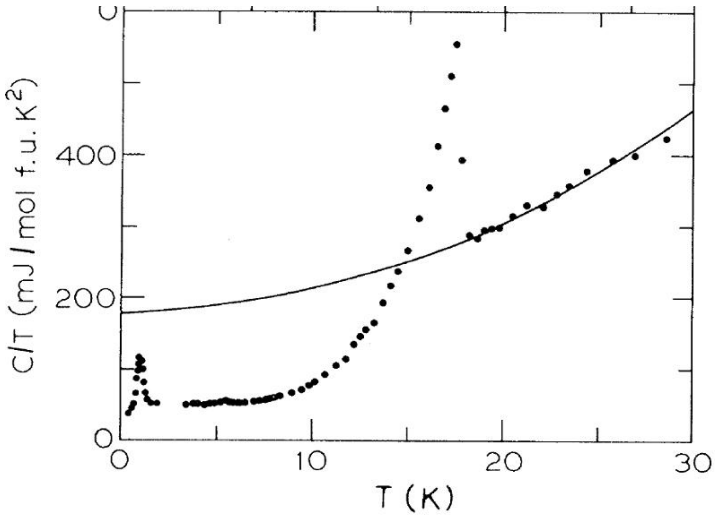

Fig. 2.2 : Specific heat C/T of polycrystalline URu_2Si_2 sample [21].

ple), susceptibility and magnetization at ambient pressure and found two large anomalies in all these macroscopic properties. The anomaly at $T_0 = 17.5$ K was interpreted as transition to antiferromagnetic order and the anomaly at $T_{SC} = 1$ K as transition to a superconducting state. In figure 2.2 is shown the specific heat C/T with the two large anomalies. The line is a $\frac{C}{T} = \gamma + \frac{12\pi^2 N k_B}{5T_D^3}T^2$ fit to the high temperature data with a Debye temperature of $T_D = 312$ K. The y-axis intercept gives the γ value. One can see that it drops during the transition from ~ 180 mJ/molK^2 at $T \sim T_0$ to ~ 60 mJ/molK^2 at ~ 2 K. This corresponds to an entropy change of $\Delta S \approx 0.2$ Rln 2. Furthermore there is a Schottky anomaly at ~ 60 K beyond the presented temperature scale.

Figure 2.3 shows the dc-susceptibility χ_{dc} of a single crystal measured along the two different crystallographic axes [21]. The response is highly anisotropic with the easy axis $\vec{c}$ and little magnetisation along $\vec{a}$. The large anisotropy implies that magnetism is understood on the basis of localised moment picture. The Curie-Weiss fit for the high temperature data $1/\chi_{dc}$ (crosses) indicates an effective moment of 3.51 μ_B with a Curie-Weiss temperature $\Theta_{CW} = -65$ K. The data derivate from the Curie-Weiss behaviour already at 150 K. The value of the dc-susceptibility at 300 K is 30 times larger than the value for the non-magnetic analogue $ThRu_2Si_2$ [32].

The resistivity is also anisotropic (see figure 2.4 [33]). Its behaviour for $I \parallel a$ has five regions:

- At high temperature the resistivity is determined by the Kondo effect with a $\rho \propto -ln(\frac{T}{T_K})$ behaviour. Here the uranium atoms present the magnetic impurities.

- Below the large maximum at $T_m \approx 75$ K the resistivity decreases dramatically due to coherence effects in a Kondo lattice. The quasi-particle band is formed.

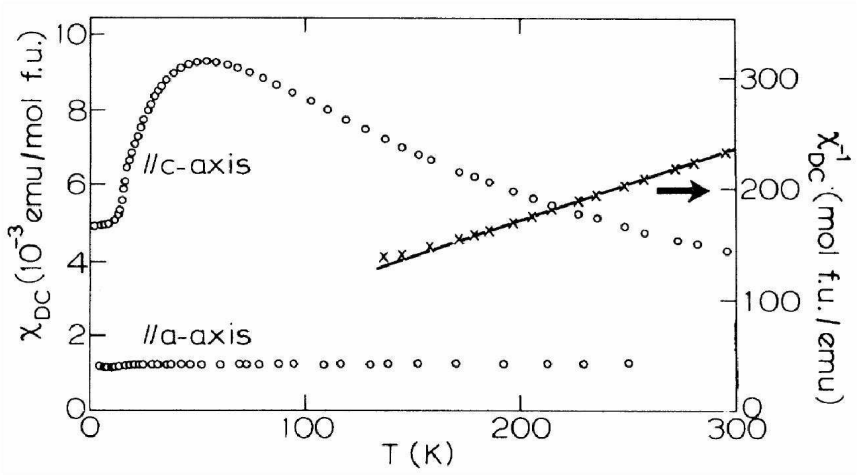

Fig. 2.3 : Dc-susceptibility χ_{dc} of a monocrystalline URu_2Si_2 sample along $\vec{a}$ and $\vec{c}$ direction in a field of $\mu_0 H = 2$ T. The line is a Curie Weiss fit of the high temperature $1/\chi_{dc}$ data (crosses) along the c axis [21].

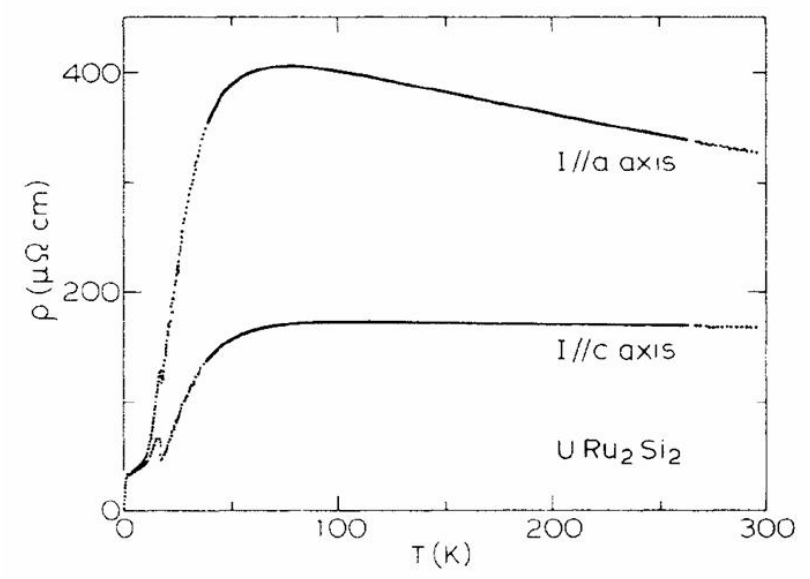

Fig. 2.4 : Resistivity of a monocrystalline URu_2Si_2 sample along $\vec{a}$ and $\vec{c}$ direction [33].

- At T_0 the resistivity curves in both crystal directions show a remarkable transition like the in spin density wave itinerant antiferromagnet chromium with an evident loss of carrier density causing a jump in resistivity.
- Below T_0 the resistivity can be accurately described by the theory of a an energy gap (Δ) antiferromagnet [34] with an additional Fermi-liquid T^2 term:

$$\rho = \rho_0 + AT^2 + bT(1 + 2T/\Delta)\exp(-\Delta/T) \tag{2.1}$$

  with $\Delta = 90(68)$ K parallel to the a (c) axis.
- Below $T_{SC} \approx 1.4$ K the compound becomes superconducting and the resistivity drops to zero in both crystal directions.

The transition at T_0 obviously resembles an electronic condensation process [35] with a gap opening on part of the Fermi surface. The specific heat data can also be nicely fitted with a gap-like exponential decay for temperatures between 2 K and 17 K:

$$C = \gamma T + \beta T^3 + \delta \exp(-\Delta/T) \tag{2.2}$$

This fit gives an energy gap of $\Delta = 115$ K. The slope of magnetisation dM/dT becomes larger for $T < T_0$ indicating the formation of a spin gap [36]. Optical conductivity measurements also suggest [37] a charge gap and finally thermal conductivity measurements [38] point towards a gap as well.

Neutron diffraction measurements revealed that the uranium 5f moments order antiferromagnetically along the c-axis below T_0 as shown in figure 2.1 [43]. The moments m are ordered ferromagnetically in the planes perpendicular to c and antiferromagnetically between these planes. In figure 2.5 are shown the results from different groups for the temperature dependence of the integrated scattering intensity I of the magnetic Bragg peak (for three-dimensional order $I \propto m^2 V_{af}$, where V_{af} is the antiferromagnetic volume) at $Q = (1, 0, 0)$ in reciprocal space, which is a forbidden nuclear peak. The ordered moment $T \longrightarrow 0$ is very small $m \approx 0.03 \pm 0.01\ \mu_B$ and stands in contrast to the fluctuating moment obtained from the high temperature susceptibility of $m \approx 3.5\ \mu_B$. Additionally the ordered moment depends on the sample [41]. The small ordered moment cannot account for the large entropy loss at T_0 that we see as jump in the specific heat if we apply the following formula [44]:

$$m_0^2 = 2\chi(T_N) \int_0^{T_N} C(T)\, dT \tag{2.3}$$

UPt_3 in comparison has a similar moment of $m = 0.02\ \mu_B$ in the antiferromagnetic phase below $T_N = 5$ K but it shows no anomalies at the magnetic transition in macroscopic properties [45, 46].

No anomaly is found in the neutron scattering intensity on the Bragg peak (1, 0, 0) at the superconducting transition, hence the antiferromagnetic phase is also present below

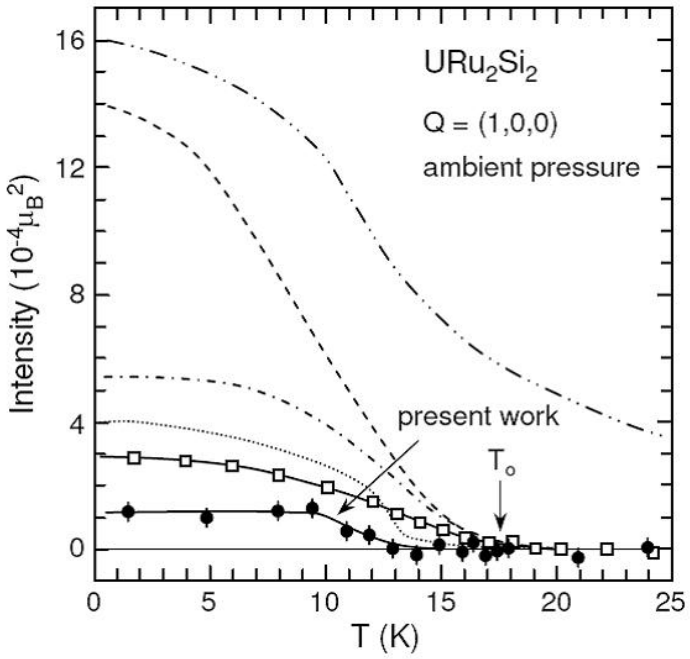

Fig. 2.5 : Neutron scattering intensity of the magnetic bragg peak of URu_2Si_2 at $Q = (1, 0, 0)$ as a function of temperature from reference [39]. Data is from [39] (closed circles), [23] open squares, [22] dash-double-dotted line, [40] (broken line), [41] (dash-dotted line), [42] (dotted line).

the transition temperature to superconductivity.

The dispersion of magnetic excitations in URu_2Si_2 in the antiferromagnetic phase is shown in figure 2.6. There are two minima with the propagation vectors (1, 0, 0) and (1.4, 0, 0). Note that the points (1, 0.4, 0), (1.4, 0, 0), (0.6, 0, 0) are equivalent on the Brillouin zone. The sharp spin waves in (1, 0, 0) direction are gapped with $\Delta \approx 1.8$ meV and in (1, 0.4, 0) direction with $\Delta_2 \approx 4.8$ meV. Above T_0 the itinerant-like spin excitations with incommensurate wave vector $Q = (1, 0.4, 0)$ are highly damped (i.e. very large) and the gap is closed. Nevertheless their integrated intensity is constant for $T > T_0$ and decreases exponentially below T_0 with a characteristic temperature of (110±10) K, the same as the gap from the specific heat [47]. Broholm *et al.* found no transverse excitations with energies up to 400 K. This explains the anisotropy of the susceptibility below 300 K.

Superconductivity coexists with the hidden order state and can give us a hint about the unknown order parameter. Only electrons which are left on the Fermi surface during the condensation process at T_0 can participate in the Cooper pair condensation process. In the specific heat the transition is seen at about 1.2 K (from the equal entropy fit) and in resistivity it is found at a slightly higher temperature (1.5 K) if the criterion is the temperature where the resistivity has dropped by half. The transition can have a double

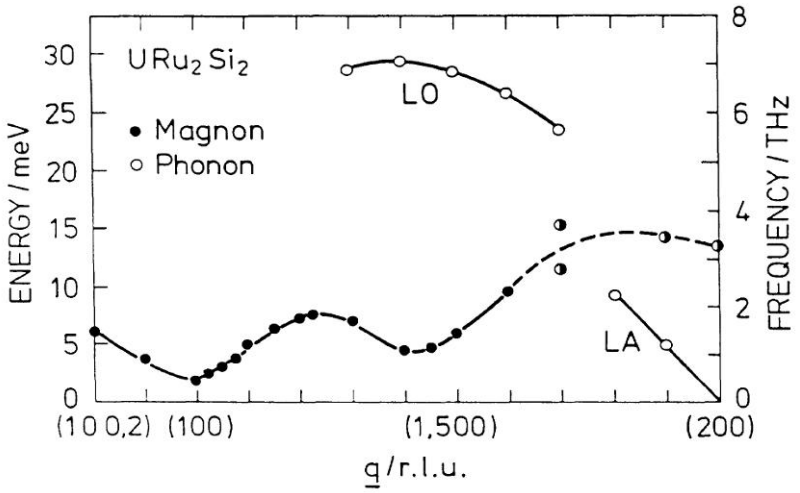

Fig. 2.6 : Dispersion of magnetic (full circles) and phonon (open circles, linear optic phonons LO, linear acoustic phonons LA) excitations of URu_2Si_2 along (ξ, 0, 0) and partly (1, 0, ξ) at 4.2 K. Half filled circles denote a hybridised exciton-phonon mode [43]. Lines are guides to the eye.

or triple step, depending on the sample and its heat treatment. In contrast to the double transition in UPt_3 this is not intrinsic and not present in every sample. The upper critical field is anisotropic (see figure 2.7) and large [21] with a value of about ~ 13 T for $H \parallel a$. But it can be described taking into account both orbital and Pauli-limitation (fit line). The upward curvature for small fields could be due to multi band effects like proposed for $PrOs_4Sb_{12}$ [48] or anisotropic pairing [49], but this unconventional behaviour is still not understood. The de Haas van Alphen frequency is the same in the normal and the superconducting mixed state but the cyclotron mass decreases in the superconducting state [51] when the field is reduced.

Theoretical models for the hidden order state are quite varied and can be basically divided into two groups [39]. In group (A) the order parameter is a magnetic dipole and the antiferromagnetism is an intrinsic property of the hidden order phase whereas in group (B) the order parameter is some other degree of freedom. In this case antiferromagnetism is not intrinsic but an additional order parameter. In the first group we include for example crystalline electric field effects [52], dynamically phased order parameter [53], spin density waves [54] or combination of local and itinerant magnetism [55]. To group (B) belong amongst others quadrupolar [56, 57] or octupolar ordering [58], unconventional density waves [59], helicity order [60], orbital antiferromagnetism [61] or Jahn-Teller distortion [62]. In group (B) two possibilities arise: i) The additional hidden order parameter can induce antiferromagnetic order, that means as soon as the hidden order parameter is larger than zero for $T < T_0$ the antiferromagnetic order parameter is automatically also different from zero. In this case the system is ordered homogeneously with two coexisting

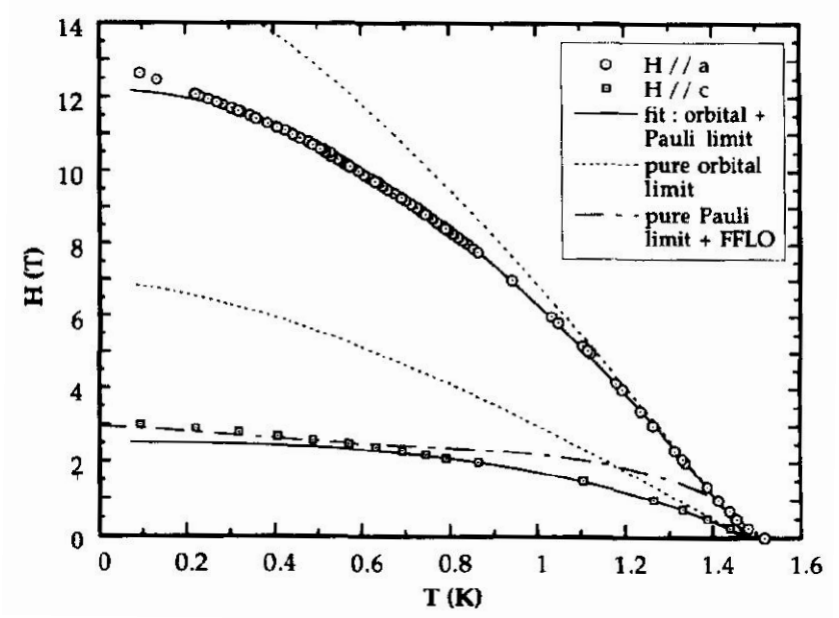

Fig. 2.7 : Upper critical field $\mu_0 H_{c2}$ of URu_2Si_2 for H ∥a and H ∥c [50]. Dashed lines are from pure orbital limit calculations and dashed-dotted lines from BCS- Pauli limit.

orders. ii) The second order is phase separated from the antiferromagnetic phase and the order parameters are not coupled. Here the volume is inhomogeneously divided between the two phases.

2.2 URu_2Si_2 under pressure

Measurements under pressure shed new light on the hidden order transition. The antiferromagnetic phase is stabilised under hydrostatic pressure which is manifested by an enhancement of the transition temperature T_0 [63, 27, 64]. The temperature dependence of resistivity under different constant pressures and the pressure phase diagram established from these measurements are shown in figure 2.8. T_0 grows first slowly up to $p \sim 1.4$ GPa (= 14 kbar) and then faster with a steeper slope. The temperature of the maximum also increases with pressure and the superconducting transition temperature decreases until ~ 1.2 GPa. When normalised to the maximum temperature and maximum resistivity, the different curves coincide accurately down to T_0. Hence the mechanisms responsible for the temperature dependence stay approximately the same under pressure. Remarkably the typical nesting shape of the resistivity is resistant to pressure.

Amitsuka *et al.* observed in 1999 a large moment antiferromagnetic phase emerge under hydrostatic pressure [23]. The neutron scattering intensity of the magnetic Bragg peak at (1, 0, 0) increased gradually up to a large saturated value of the moment of $m \approx 0.4\ \mu_B$ for $p \gtrsim 1.4$ GPa. This value would account for the entropy change at T_0 at zero pressure. However the entropy change at high pressures is not known. High

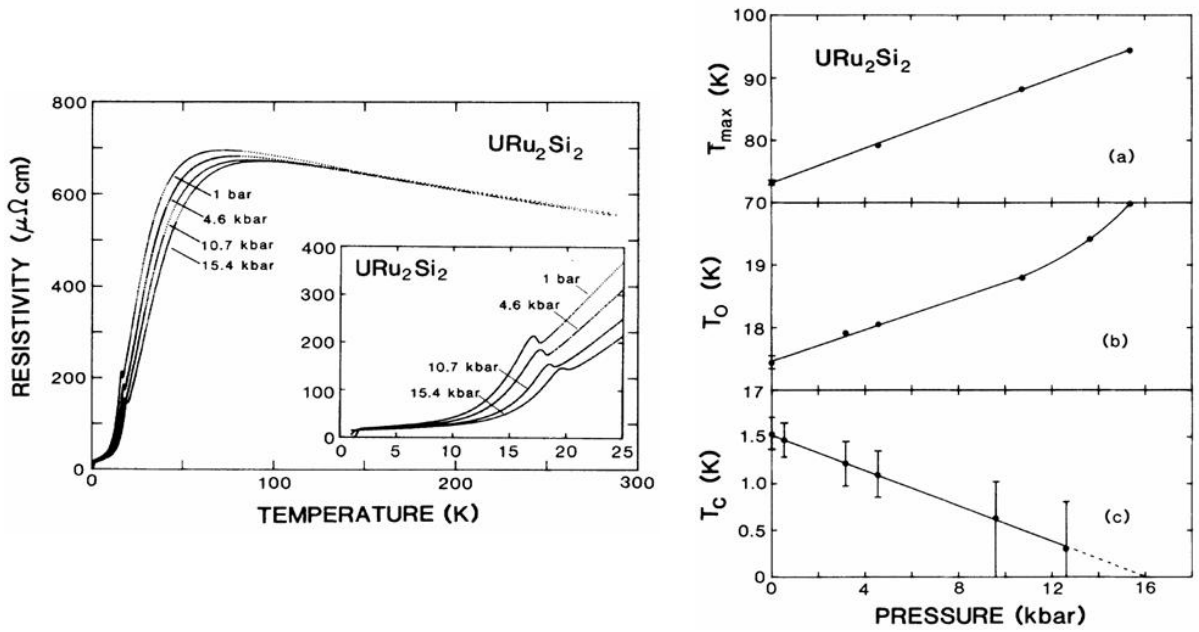

Fig. 2.8 : Left side: Temperature dependence of resistivity of URu_2Si_2 for the pressures 0.1 GPa, 0.46 GPa, 1.07 GPa and 1.54 GPa [27]. Right side: Pressure phase diagram from these measurements[27].

pressure ^{29}Si-NMR [65](nuclear magnetic resonance) and μSR [25](muon spin resonance) measurements indicated that it is not the magnetic moment but the volume fraction of the antiferromagnetic phase which increases with pressure at the expense of the hidden order phase. In contrast to neutron scattering, where a volume average is measured (scattering intensity $I \propto m^2 V_{af}$) these two methods can distinguish the volume fraction and the ordered moment. In nuclear magnetic resonance the volume fraction is given by the intensity of the resonance line and its Larmor-frequency is proportional to the Zeeman-splitting in the local field. At low temperature with increasing pressure the frequency of the antiferromagnetic resonance lines does not change, only their intensity grows (see the two outer peaks in figure 2.9). This means that the local field at the Si sites created by the uranium moments stays the same, only the number of Si atoms located in field and consequently the magnetically ordered volume grows. Over a wide pressure range (0.1 GPa - 1.52 GPa) the paramagnetic phase (seen as the line in the middle) is also present next to the antiferromagnetic phase but the two phases are locally seperated.

From thermal expansion measurements Motoyama *et al.* [24] found a sharp steep transition line between the hidden order and the large moment antiferromagnetic phase (see figure 2.10). This is in contrast to the quite large pressure range, in which the volume of the antiferromagnetic phase increases in first measurements by Amitsuka *et al.* and in NMR by Matsuda *et al.* They suggested therefore a first order phase transition in the pressure phase diagram and ascribed the large transition pressure ranges to inhomogeneous pressure in those measurements. They measured the thermal expansion with the

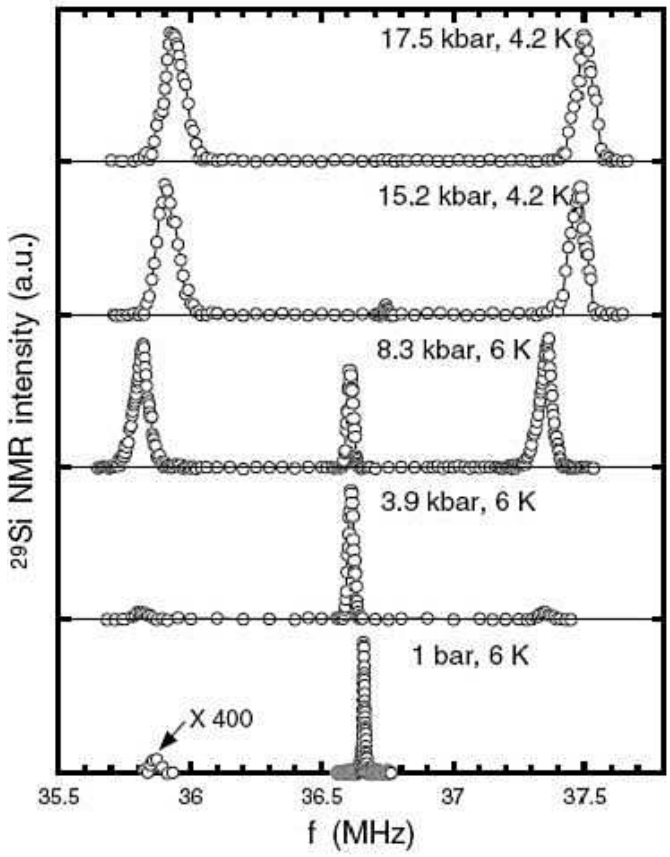

Fig. 2.9 : NMR spectra of URu_2Si_2 for different pressures [66] at low temperature. The frequency of the central resonance line is slightly shifted for different pressures because the field in which the spectra were taken varied between the measurements.

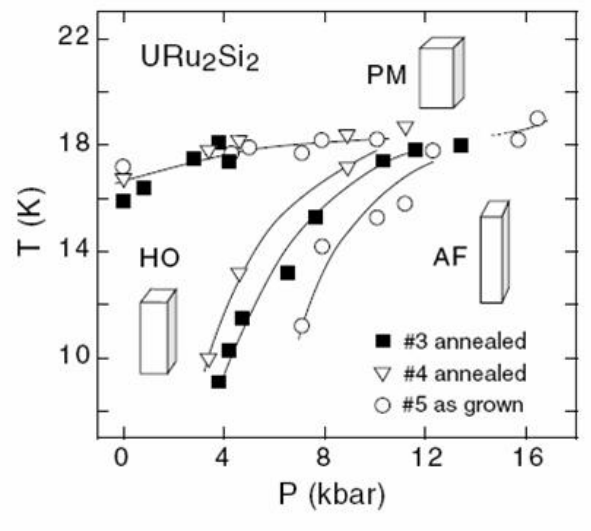

Fig. 2.10 : Pressure phase diagram of URu_2Si_2 from thermal expansion [24] from three different samples. The transition line between hidden order and antiferromagnetism is measured for three different samples.

strain gauge method. The data at zero pressure correspond nicely to the data by deVisser *et al.* [67] who used a capacitive method. In their data presented in figure 2.11 at 0 GPa and 0.5 GPa only the transition at T_0 is visible. With pressure it moves to higher temperatures. The second peak at T_x is very clearly coming up at $p > 0.71$ GPa and also shifts to higher temperatures. Whereas the transition at T_0 attenuates with pressure, the new transition seems to survive to higher pressures. Its shape seems to change from gaussian like to a mean field like discontinuous jump for 1.64 GPa when only one transition is left. The c/a ratio increases at the transition to large moment antiferromagnetism. For different samples the transition line between hidden order and antiferromagnetism occurs at different pressures with a lower critical pressure for the annealed samples having a higher superconducting transition temperature.

Yokoyama *et al.* carried out neutron scattering measurements under uniaxial stress [26]. The ordered moment increases very sensitively for pressure applied along (1, 0, 0) and (1, 1, 0) and not for pressure along (0, 0, 1). Bakker *et al.* also prooved that T_0 increased only under uniaxial stress $\sigma \parallel$a and decreased for $\sigma \parallel$c [68]. The ratio $\frac{c}{a} \equiv \eta$ is the key parameter which drives the transition from hidden order to antiferromagnetism. Its critical value η_c is very small. This is proposed to be the reason, why the antiferromagnetic phase can appear locally, where lattice defaults cause internal strains with values of $\eta > \eta_c$ even at ambient pressure. In this case the antiferromagnetism measured by neutron scattering at ambient pressure would be parasitic in a very small valume fraction (~ 0.6 %) in the non-magnetic hidden order phase.

So far, experiments under pressure support a theory with two order parameters: the

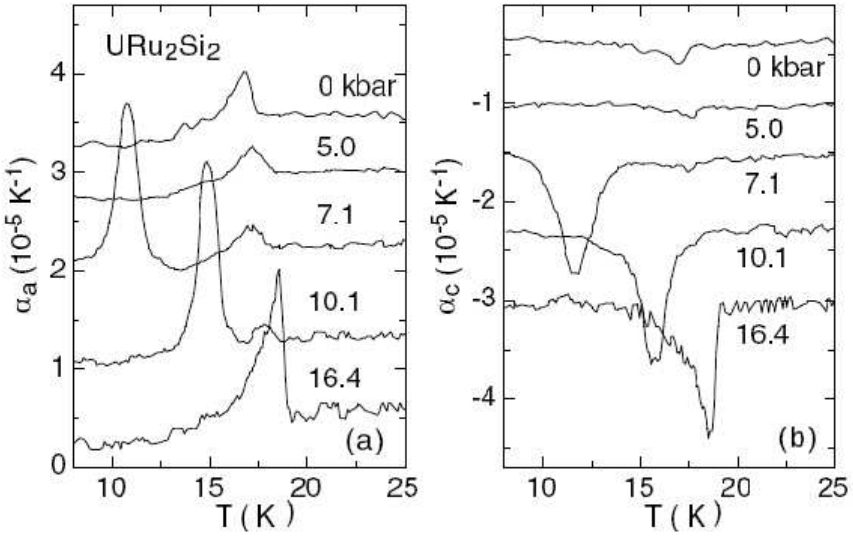

Fig. 2.11 : Temperature dependence of the thermal expansion coefficient of URu_2Si_2 in the two crystal directions for sample #5 at different pressures [24].

hidden order parameter (now called Ψ) giving rise to the large anomaly in the specific heat and the large moment antiferromagnetic order parameter m. Possibilities for the hidden order parameter are given in the end of paragraph 2.1. A phenomenological framework to study the pressure-temperature phase diagram presents the Ginzburg-Landau theory. The topology of the pressure phase diagram is important for the symmetries of the concerned order parameters [54, 69, 70]. Up to now the calculations have only been done for the case of a homogeneous distribution of both order parameters over the entire sample volume (group B, case i) [54]. For such a system the one dimensional Landau functional for the free energy density is given as:

$$f = \alpha_\Psi \Psi^2 + \alpha_m m^2 + 2\gamma \Psi m + \beta_\Psi \Psi^4 + \beta_m m^4 + 2\beta_i \Psi^2 m^2 + ... \qquad (2.4)$$

The topology of the pressure phase diagram depends strongly on the existence of the third term that means on $\gamma = 0$ or $\gamma \neq 0$. If $\gamma \neq 0$ a linear coupling between the two order parameters is possible. This can only be the case, if both of them break the same symmetries (e.g. lattice translation, time reversal). The order parameters develop below $T_0(p)$. A first order transition line occurs between the hidden order and the antiferromagnetic phase, if $\beta_i > \sqrt{\beta_\Psi \beta_m}$, i.e. in case of strong microscopic repulsion between the two order parameters. Equation 2.4 gives then two different phase diagrams presented schematically in figure 2.12.

If $\gamma = 0$ (left panel) one finds two separated regions on the pressure-temperature phase diagram. At low pressure below the transition line at T_M (in this work called T_x), only the hidden order parameter Ψ is greater than zero and no magnetic moment exists, whereas at high pressure there is no hidden order and only antiferromagnetic order. The transition line at T_M joins the second order transition lines at $T_m(p)$ (in this work called

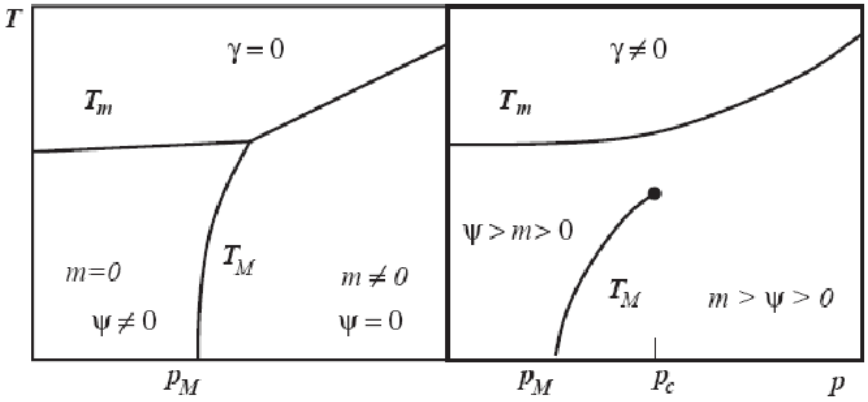

Fig. 2.12 : Schematic pressure-temperature phase diagrams of the functional in equation 2.4 for $\gamma = 0$ (left panel) and $\gamma \neq 0$ (right panel)[54].

T_x) in a bicritical point. If $\gamma \neq 0$ (right panel) both order parameters are non-zero below T_m for all pressures and both phases coexist. The first order transition line between the hidden order dominated phase at low pressure and the antiferromagnetic order dominated phase at high pressure stays seperated from the T_m transition line and ends in a critical end point.

Similar considerations yet have to be done for the case of inhomogeneously phase separated order parameters (group B, case ii).

The phase diagram by Motoyama *et al.*(see figure 2.10) is not clear concerning the question if the transition lines touch. In previous resistivity [27] and specific heat [71] measurements under pressure the transition line at T_x has not been seen at all. Bourdarot *et al.* published the phase diagram in figure 2.13. Note that the transition line at T_m is determined from resistivity measurements (black open circles) and the transition line at T_M from neutron diffraction measurements (blue closed circles). The lines don't touch below 1.3 GPa, which supports in their opinion a Landau functional with $\gamma \neq 0$ (right panel in figure 2.12). Obviously it is better to detect both transitions at the same time with the same technique to be sure that there is no problem with thermometry. This will be done in our study with the additional advantage that in our labratory very tiny pressure steps are possible so that the pressure region where the lines should touch can be scanned very carefully.

Microscopic measurement techniques like neutron diffraction, NMR and μSR reveal fundamental differences between the hidden order phase and the pressure induced large moment antiferromagnetic phase. One could expect that this implies also significant changes in macroscopic quantities notably in the signature of the transition at T_0 at low pressure (transition to hidden order) and at high pressure (transition to large moment antiferromagnetism). At first view this is not valid for resistivity measurements. There the signature of the transition at T_0 does not change apparently under pressure. The two

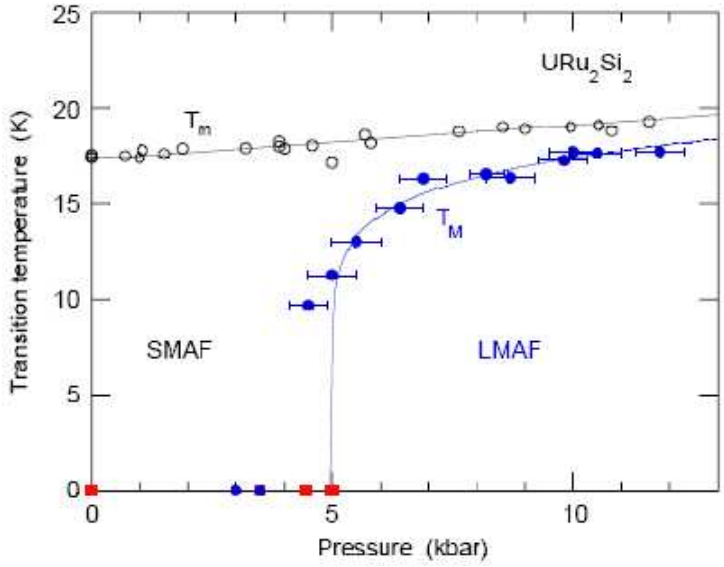

Fig. 2.13 : Pressure-temperature phase diagram of URu_2Si_2 [72]. The transition line at T_m is determined from resistivity measurements (black open circles) and the transition line at T_M from neutron diffraction measurements (blue closed circles). (closed circles for pressure clamps, closed squares for hydrostatic helium cells). The lines are guides to the eye.

phases indeed seem to be quite similar. De Haas-van Alphen experiments under pressure for example didn't show any abrupt changes of the Fermi surface at low temperature up to $p \approx 1.8$ GPa [73]. One of our main objectives in this study will be the detailed investigation of the signature of the transition at T_0 in resistivity and specific heat up to pressures of 2.5 GPa, where we are sure to be far in the antiferromagnetic phase.

As a last point in our description of previous experimental results we want to look at the pressure dependence of the superconducting transition. Concerning this question previous measurements are contradictory. Uemura *et al.* show that superconducting transition measured with ac-susceptibility is abruptly suppressed at $p \sim 0.5$ GPa [30]. Because this is the pressure where antiferromagnetism sets in they claim that superconductivity competes with the large moment antiferromagnetism. On the other hand resisitivity measurements by McElfresh [27] and Schmidt [29] show that the superconducting transition is indeed slowly suppressed with pressure but seen up to ~ 1.2 GPa (see figure 2.8) far in the antiferromagnetic phase. As resistivity in opposition to susceptibility is not compulsorily a volumic property it is possible that the superconductivity exists only on the surface or on inhomogeneous paths through the sample in the antiferromagnetic phase. The nature of the hidden order parameter of the superconductivity is still unknown and the answer to the question whether superconductivity can coexist with antiferromagnetism in this compound could give a hint about it. Specific heat measurements under pressure as carried out in this study will give us information about bulk properties. It is the appropriate means of studying the pressure dependence of the superconducting transition.

Chapter 3

Experimental methods

In order to understand the phases in URu_2Si_2, their interplay and competition, microscopic measurements (especially inelastic neutron scattering) are necessary but not yet done at high enough pressures to explore region of the large moment antiferromagnetic phase. Macroscopic measurements under pressure are therefore an important tool to determine the phase diagram and to look at the signature of the transitions at T_0 for different pressures. As well they allow a study of the behaviour of the different phases under pressure and magnetic field.

3.1 Samples

The sample quality plays a crucial role in material physics and most notably in uranium compounds where metallurgical effects can completely change the sample properties. Owing to this a careful choice of the sample is fundamental for a successful experiment. Throughout this work all measurements under pressure were done in the same pressure cell with the same sample.

3.1.1 Preparation and characterisation of the single crystals

The single crystals studied in this work were grown by Pascal Lejay at CRTBT/CNRS Grenoble. The basic materials had a very high purity: depleted uranium 99.9 %, Ruthenium 99.99 % and Silicon 99.9999 %. In a first step, these materials are melted in stoichiometric proportions U:Ru:Si = 1:2:2. The melting temperature is not measured but estimated to about $T_m = 1800$ °C. The heating is achieved by a high frequency alternating field additional to a static magnetic field which makes the drop of liquid URu_2Si_2 levitate. Nevertheless URu_2Si_2 is very reactive at high temperatures and therefore the use of a water cooled copper melting crucible is required. Moreover the melting is done under purified Argon atmosphere to avoid UO_2 being formed. It's not possible to work in vacuum because all the Silicon would volatilize.

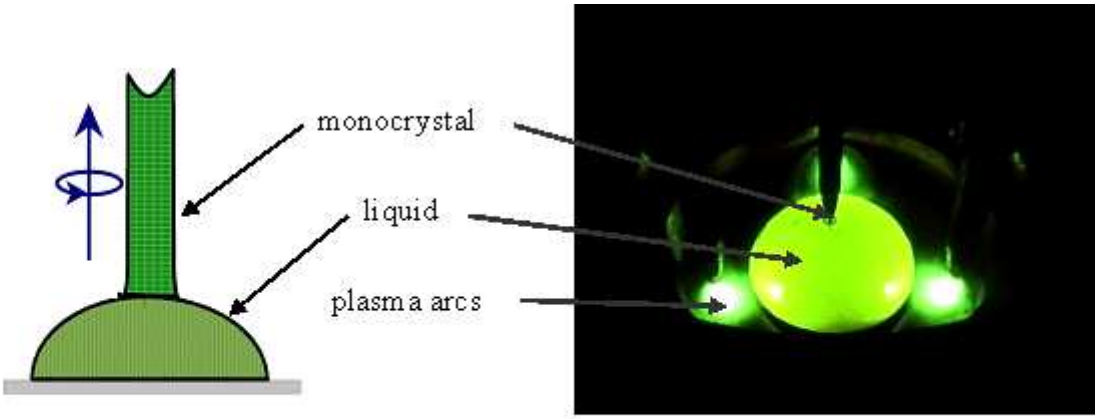

Fig. 3.1 : Czochralski method and photo of a tri-arc furnace in action.

Using x-ray scattering the structure of the polycrystalline samples is tested and no parasitic phases could be found. The monocrystal is pulled by Czochralski method in a tri-arc furnace (see figure 3.1). For this the polycrystal is put on a cooled copper plate in the furnace which is first evacuated to an ultra high vacuum in order to clean the furnace. Then again under pure Argon atmosphere of a pressure of about 1 atm the sample is melted by three Argon arcs. An oriented monocrystalline seed crystal is dipped into the liquid and pulled at about 5 mm per hour. A rotation of about 20 turns per minute homogenises the temperature. The single crystal can have a diameter of about 5 mm and a length of several centimetres.

The four samples that were at my disposal were precut by electro erosion and already small with masses of $\sim$ 1 mg. The sample out of which I cut my small sample for the pressure cell is called sample #2 here. Its mass is about $m \approx 0.8$ mg and it had the dimensions $1200 \times 600 \times 150$ $(\mu\text{m})^3$. Its specific heat was measured in a commercial Quantum Design Instrument PPMS down to $T = 0.4$ K. Compared to samples 1, 3 and 4 it has the most prominent anomaly at the superconducting transition (see figure 3.2a) although it shows a slight double step feature. This is the reason why I continued my work with it. Note that the form of the transitions at T_0 and T_{SC} seems to be correlated. Additionally this sample had the right size to be cut and polished by circular saw. With a 15 μm thick saw blade covered with diamond powder first a 100 μm thick slice was cut. It was then cut into two halves and one of the little ashlars was polished on two sides to its final size of $283 \times 60 \times 50$ $(\mu\text{m})^3$ (see figure 3.3). These lengths are measured with a micrometric screw under microscope and the error is about $\Delta l \approx 3$ μm. In order to know the orientation of the mini crystal, I made a Laue diagram of the larger sample #2. The current injection for the resistivity measurements is finally not parallel to any crystal axis. In polar coordinates the angles to the c-axis are approximately $\Theta \approx (25 \pm 2)^\circ$ and $\phi \approx (7 \pm 2)^\circ$. This sample will be called sample 2a in this work. In literature better samples with a higher transition temperature T_{SC} are known (see for example [74]).

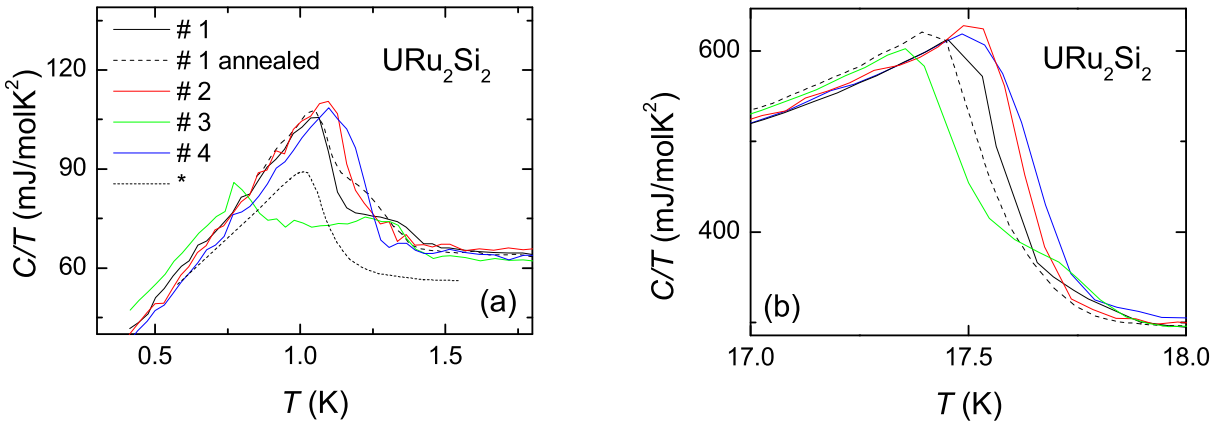

Fig. 3.2 : The specific heat at the superconducting transition (a) and at the transition at T_0 (b) of different samples before choosing sample #2 to proceed. $*$ The short dashed line in (a) gives the specific heat C/T of the best sample measured by Motoyama *et al.* [24]

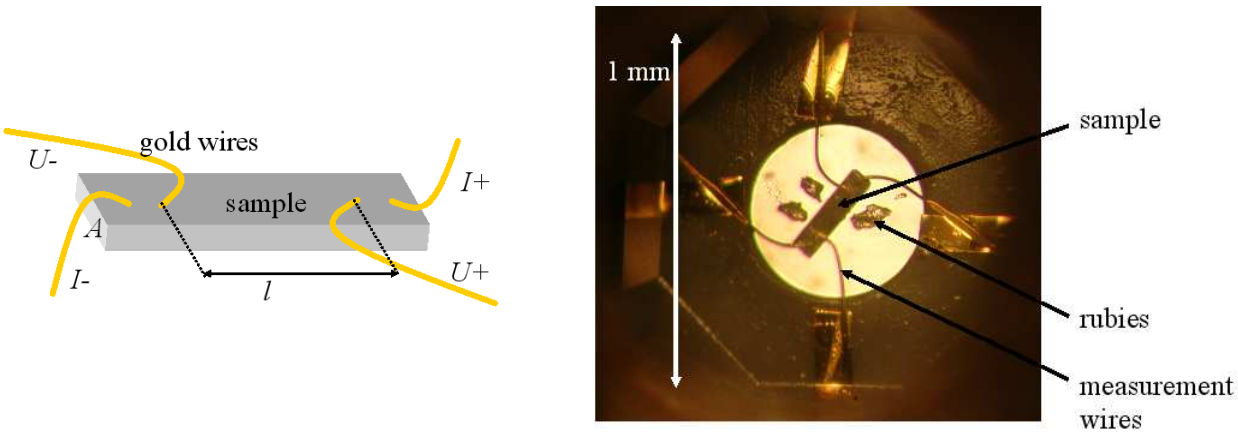

Fig. 3.3 : a) Scheme of resistivity measurement setup with four point contact method. b) Photo of realisation in pressure chamber.

3.2 Resistivity measurements

The resistivity ρ is measured via the four point contact method presented in figure 3.3. Four gold wires with a diameter of 10 μm are welded on the sample, the outer ones for the injection of the measurement current I and the inner ones for the voltage measurement U. The resistivity is then calculated according to the formula

$$R = \frac{U}{I} \quad R = \rho \frac{l}{A} \quad \Rightarrow \rho = \frac{U}{I}\frac{A}{l} \tag{3.1}$$

with the cross sectional area A and the distance l between the inner wires. A Stanford SR830 Lock In amplifier serves as alternating voltage source. A tension of $U = 1$ V through a $R = 10$ kΩ resistance delivers a current of $I = 100$ μA. The resistance of the cables and the sample can be neglected compared to this resistance even though the cables for current injection are superconducting wires with a large resistance above the transition temperature. This is proven by the fact that no jump is detected in the

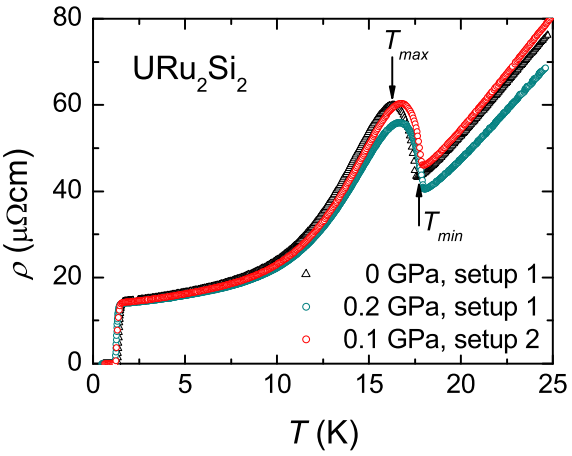

Fig. 3.4 : Comparison of temperature dependence of resistivity at low pressure between setup 1 and setup 2.

measurement signal. The measurement frequency is 17 Hz. The measurement signal is amplified first by a transformer by a factor of 100 and second by a Stanford SR560 low noise pre-amplifier by a factor of 1000 and then measured by the same Lock In. The error on resistivity is mainly due to the uncertainty of the geometric factor $\Delta(\frac{A}{l}) \approx 8$ %. This is a systematic error, basically just a wrong normalisation factor. As it is the same factor for all pressure curves for one pressure cell setup the resistivity curves measured with one cell setup can be compared in a more precise way.

During this work, I measured two resistivity setups. In setup 1 measurements from 0 GPa to 1.78 GPa were carried out in the ^{3}He cryostat and measurements with very small pressure steps from 0.3 GPa to 2.4 GPa in the ^{4}He cryostat. The geometrical factor $\frac{l}{A}$ for the first setup is given by the distance between the welding points of the inner wires of about $l = 154 \pm 3$ μm and the cross section of the sample of $A = 50 \times 60$ $(\mu\text{m})^3$.
In the second setup, the distance between the welding points was $l = 163 \pm 3$ μm with the same cross section. The measured pressures are 0.1, 2.28, 3.45, 4.37 and 5.37 GPa. Apart from the lowest pressure, I had a short circuit between one measurement wire for current injection and the cell body and at the highest pressure even between two measurement wires and the cell body. This is the reason why the signal was very small and noisy and the normalisation factor was higher. I basically only determined the transition temperatures at T_0 from these measurements which were clear despite the short circuit. The temperature dependence of the resistivity from the second setup compared to the first one is slightly different even at low pressure, notably in proximity to T_0 (see figure 3.4). The transition temperature at 0.1 GPa of setup 2 (red) is between the transition temperature of setup 1 at 0 GPa (black) and 0.2 GPa (green), but the height of the jump in resistivity, defined as $\rho(T_{max}) - \rho(T_{min})$, is smaller. Because this hight depends

sensitively on the crystal direction (see figure 2.4), the different geometry i.e. slightly different angles in current injection and voltage measurement in the two setups caused the different heights. One can say, that in setup 1 the resistivity is measured more in the c direction.

3.3 Ac-calorimetry under pressure

For an ideal specific heat measurement, the sample must be thermally isolated from its environment. Then a certain known amount of energy is added increasing the inner energy of the sample by ΔU and the temperature enhancement of the sample ΔT is determined. The specific heat C is calculated with the formula $C = \frac{\Delta U}{\Delta T}$ for $\Delta T \longrightarrow 0$. In a pressure cell the sample is thermally strongly coupled with the Argon bath and the measurement wires. The coupling most probably depends on temperature and pressure and is not well known. Therefore we use the ac-calorimetric method described more detailed in [75, 76]. In this method the sample is heated with an alternating power $P = P_0(1+cos\omega t)$ where P_0 is the mean value and ω the oscillation frequency. The induced temperature oscillations T_{ac} of the sample are then measured with a thermometer. The coupling with the environment is taken into account as a heat leak with thermal conductance κ . A detailed description is given in reference [77].

The sample temperature consists of several terms:

$$T = T_b + T_{dc} + T_{ac}\cos\omega t \tag{3.2}$$

with the temperature of the bath T_b, the average temperature enhancement due to average heating $T_{dc} = \frac{P_0}{\kappa}$ and the temperature oscillation $T_{ac}\cos\omega t$ with the same frequency as the heating and the amplitude T_{ac}. Thus we obtain

$$T_{ac}e^{i\phi} = \frac{P_0}{\kappa + i\omega C_{ac}} \tag{3.3}$$

Φ is the phaseshift between the heating and the T_{ac} signal. The measurement frequency has to be chosen high enough to decouple the sample from its environment i.e. $\omega C_{ac} \gg \kappa$, but not so high that the heat is not distributed homogeneously in the sample. In this case we obtain for the specific heat C_{ac} of the sample in dependence of the measured temperature oscillations T_{ac}

$$C_{ac} = \frac{P_0}{\omega T_{ac}} \propto \frac{1}{T_{ac}} \tag{3.4}$$

In our setup the sample is heated with a laser diode beam lead into the cryostat via optical fibres. The laser diode is controlled by the Lock In amplifier.

The used thermometer is a thermocouple Au:Au(0.007% Fe) with a thermoelectric power $S = \frac{\Delta U}{\Delta T}$. The sensitivity was measured by Chaussy *et al.* [78] and has at one Kelvin the value of $S(1\text{K}) \approx 7\ \mu\text{V/K}$. It is assumed to be independent of pressure [79].

The measurement signal is the ac-part of the thermocouple voltage $V_{ac} = ST_{ac}$ and its phaseshift to the heating. Like for the resistivity measurement the signal is amplified by a factor of 100 with a transformer and by a factor of 1000 by a pre-amplifier. It is then read out by the Lock In with the same as the excitation frequency.

Up to this point we would be able to determine the absolute value of the specific heat, but in reality this is not the case: Due to the tiny size of our sample not only the sample but also the environment is heated by the laser beam as it is not well focused. This is the reason why P_0 i.e. the average heating power and the amplitude are unknown and they change when the setup is moved and for example connections of the optical fibers are changed. As a consequence, the absolut value of the specific heat is not known. Another mistake comes from the fact that we measure not only the sample but also its environment. This gives us a pressure and temparature dependent background signal. As κ grows with temperature, the chosen frequency (which fulfils the condition $\omega C_{ac} \gg \kappa$) is small ($f = 127$ Hz) at low temperature when the superconducting transition is measured and higher ($f = 678$ Hz) for the measurement at higher temperature.

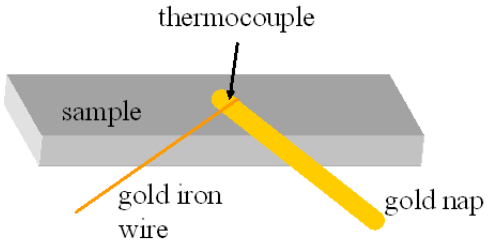

Fig. 3.5 : Schematic ac-calorimetry setup. Gold–gold/iron thermocouple welded to the sample.

The last problem that has to be mentioned here is the fact that the sample has an average temperature which is elevated in comparison to the bath. This elevation (T_D) is not known as we measure only the absolute temperature of the bath T_B with a thermometer on the outside of the pressure cell but it is proportional to the heating power ($T_D = \frac{P_0}{\kappa}$). Since the temperature of the sample, which is unknown, is higher than the temperature of the thermometer, we see the transition at a lower temperature. The absolute temperature of the sample and therefore T_D could be determined by measuring the dc voltage of the thermocouple. Another method, and this is the one used in this study, is to trace the transition temperature as a function of the heating power. A linear extrapolation to zero power will then give the real transition temperature because in this limit T_D is zero. This effect is taken into account when looking at the superconducting transition but not at the transition at T_0 since $T_D \ll T_B \approx T_0$.

Because of the unknown P_0 and background this method is –strictly seen– only qualitative. It allows us to determine the transition temperatures where the specific heat makes a jump and to draw that way the phase diagram for different pressures. But it is known from previous measurements of e.g. $CeRhIn_5$ that this technique gives reliable even semi-quantitative data in the pressure region up to ~ 4 GPa [80].

3.4 Pressure

Pressure is a controllable and reversible tool for tuning sample size and lattice parameter. Along with chemical doping and magnetic field it changes the hybridisation in heavy fermion compounds and can induce a quantum phase transition. Contrary to chemical substitution which leads to disorder effects, pressure is a clean method to change the lattice parameter with the slight disadvantage that negative pressures are not procurable. In our case, negative pressures are not required as the interesting pressure region is in particular between 0 and 2.5 GPa.

Working under high pressure is experimentally difficult for several reasons: Since pressure is defined as

$$p = \frac{F}{A} \qquad [p] = \text{GPa} = 10\,\text{kbar} = 10^9 \frac{\text{N}}{\text{m}^2} = 10^9 \frac{\text{kg}}{\text{ms}^2} \tag{3.5}$$

high pressure requires a large force F on a small surface A. For this reason pressure chamber and hence sample sizes are very small which implies on the one hand a work under microscope when preparing the sample and the cell and on the other hand a small signal. But the enormous advantage of heavy fermion systems is their large macroscopic quantities at low temperature as the specific heat and resistivity. Consequently the signal is detectable in spite of the tiny sample size. Another difficulty is to introduce the measuring wires into the pressure chamber without loosing leak tightness: Typical gaskets are made out of stainless steel. The measuring wires have to be electrically isolated against it to avoid shorted currents while the setup has to stay leakproof. This technique is well established in the laboratory and described in paragraph 3.4.2. Additionally pressure is not a continuous variable and measurements are usually temperature scans at constant pressure. The change of pressure is implemented at room temperature (for measurements in^{3}He cryostat) and pressure reduces upon cooling between 0.5 GPa and 1 GPa but below $T = 50$ K it doesn't change significantly[81]. Measurements are usually made at constant pressures. It is hard to achieve the desired pressure at low temperature because the cell doesn't behave linearly due to mechanical relaxation processes during cooling.

A large variety of different pressure cells exist, for example piston-cylinder pressure cells, Bridgman cells and diamond anvil pressure cells. In this study a diamond anvil cell was used which can attain pressures up to 20 GPa.

3.4.1 Pressure cell

The cell I used for most of my measurements is a diamond anvil cell (see figure 3.6). It is made out of CuBe with anvils made out of the hardest material known, diamond. Two flat diamond anvils with a table diameter of $d = 1$ mm are glued to the pistons. They are aligned coplanar with the help of Newton rings. One of the pistons is fixed to the outer cylinder, the other one can be moved by turning three screws in order to apply

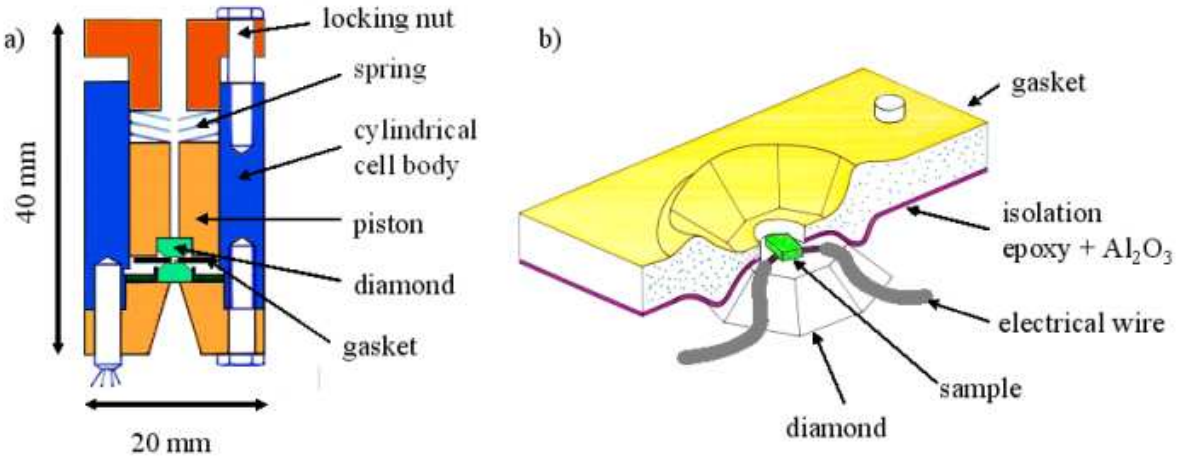

Fig. 3.6 : Diamond anvil pressure cell (a) and gasket (b) as used in this work.

or to change the pressure. The mobile piston is well guided along the symmetry axis in the cylinder with the help of a groove to avoid inhomogeneous pressure on the diamonds which could make them break. The two diamonds exert pressure on a gasket with a hole, the pressure chamber, filled with the pressure transmitting element. The sample swims in this liquid and receives the same force from all directions.

Due to the large forces a pressure cell setup can fail at several stages: During loading the failure rate is about 3/4. Frequent heating and cooling works on the wires and can break them. And last but not least the pressure chamber is deformed when the pressure is changed. This can induce a breaking of the wires and also short circuits, when the wires or the sample touch the gasket.

3.4.2 Gasket

A key point to a successful pressure cell setup is the gasket. The pressure cell is first mounted with the gasket only. By applying a force of about 8000 N the gasket is preformed until the thickness of it between the diamonds is about 100 μm. In the centre of the diamond impression a hole is drilled by hand with a diameter of 500 μm. This presents the pressure chamber (see figure 3.6). The insulation between gasket and measurement wires is assured by a thin layer of epoxy glue (stycast) mixed and saturated with Al_2O_3 powder. Only that way it has the required rigidity and strength to resist high pressure. On four sides of the diamond there are contacts for the measurement wires. Flattened 25 μm gold (or gold-iron for the thermocouple) wires are glued to these contacts with silver paste and attached perpendicularly to the diamond anvil. They are cut on the anvil table so that they don't enter the pressure chamber. Then the small 10 μm gold wires are contacted to the sample by spot welding. Typical welding parameters for my sample were a voltage of U = 4 V and a time constant of $\tau = 9$ μs. For the resistivity setup the four wires must be bent all in the same direction before welding leading to the flexibility

needed when the pressure chamber is deformed. Otherwise the wires or the bond would break. Finally the sample is placed on the diamond as seen in figure 3.6. The small wires are pushed under the broad wires arriving from the outside. The contact is achieved only under pressure when the cell is loaded. Next to it some rubies are arranged which will be necessary for the pressure measurement. In figure 3.3 a resistivity setup is photographed through the (unloaded) pressure cell with the help of a microscope. The diamond, sample in the pressure chamber, small wires, broad wires and the rubies are discernible.

3.4.3 Pressure transmitting element

In this laboratory we use Argon as pressure transmitting element. The noble gases and especially Helium are the most adequate media because they are highly isotropic. The only interactions between the atoms are van der Waals forces which are non-directional. The enormous disadvantage of He is its high compressibility at low temperatures which induces large changes of the pressure volume. This causes problems with the measurement wires in the pressure chamber due to deformation. Argon is also highly hydrostatic at least up to 10 GPa [81]. To load the cell, it is only slightly closed and plunged into liquid Argon during 45 min. After that time the cell is cold and almost no gas bubbles are formed any more. Pressurising with a force of about 5500 N induces a pressure of about 1.1 GPa at room temperature.

3.4.4 Ruby method of pressure measurement

We introduce some ruby crystals into the pressure chamber next to the sample before closing the pressure cell, which serve as pressure sensors. The wavelength of the fluorescence lines of rubies depends on pressure and on temperature. Below T$\approx$ 35 K the line position does not depend on temperature any more but only on pressure. By measuring the spectrum, we can deduce the pressure in the chamber at several positions. The rubies are excited by an Argon laser, whose light is lead to the pressure cell into the cryostat via an optical fiber. Here we benefit from the fact that the diamond anvils are transparent. The outcoming light is again lead outside the cryostat via an optical fiber on the other side of the pressure cell. It is spectral-fragmented with a HR 1000 monochromator of Czerny-Turner type. The emission spectrum is taken with an Andor Technology CCD spectrometer. At room temperature $T = 300$ K and zero pressure, two ruby lines, called R_1 and R_2 are at the positions $\lambda_{R_1} = 694.239$ nm and $\lambda_{R_1} = 692.82$ nm. With the help of these lines and a reference line from a Ne lamp the spectrometer is calibrated. Independently of temperature within an error of 3% [82] the lines shift with 0.365 nm/GPa. The pressure is measured at room temperature and at 4.2 K. At low temperature the excited state which leads to R_2 is not thermally populated and therefore the line is not detectable. In the concerned pressure region the pressure changes between 0.55 GPa and 1 GPa upon cooling. The absolute pressure error is estimated to about $\Delta p \approx 0.05$ GPa.

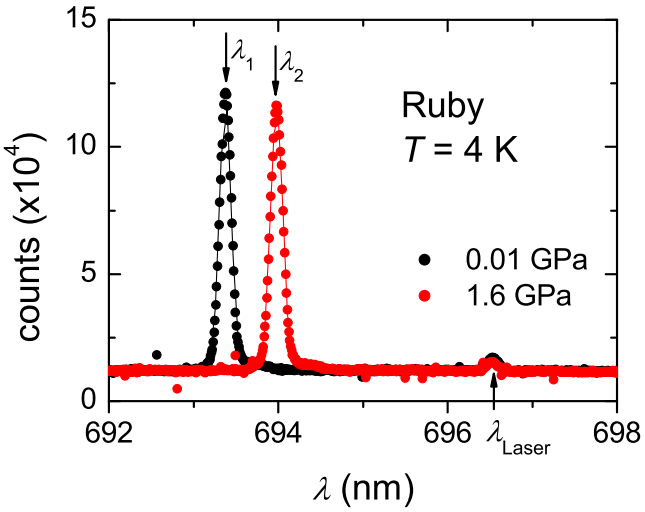

Fig. 3.7 : Ruby spectra at 4.2 K for two different pressures in cell setup 1.

We always measured the pressure at 4.2 K before the measurements of this pressure and before heating up. Within the error bar we never observed changes in pressure between these two measurements without heating up inbetween. Therefore we claim the pressure to be stable. If the pressure in the chamber is not homogeneous, the different rubies will have slightly different emission lines. This leads to a broadening of the line. Hence its width indicates the homogeneity of pressure in the chamber. In figure 3.7 the ruby spectra at 4.2 K for two different pressures in one cell setup is shown: 0.01 GPa (black dots) and 1.6 GPa (red dots). The lines are gaussian fits of the peaks with their maxima at $\lambda_1 = 693.38$ nm which corresponds to 0.01 GPa and $\lambda_2 = 693.98$ nm which corresponds to 1.6 GPa. The width of the peak in the low pressure spectrum is $0.137 \pm .0005$ nm, which es exactly the width of the peak of the rubies in the unloaded cell. For 1.6 GPa it is slightly enhanced to $0.147 \pm .0005$ nm showing a tiny loss of hydrostatic conditions. The small peak at $\lambda_{Laser} = 696.54$ nm is a harmonic of the laser. The same laser is also used at high temperature as excitation of the sample. In this case the beam is chopped by a mechanical chopper.

3.4.5 Changing pressure

During my Diplomarbeit I used basically two methods to change pressure: For the measurements in the ^{3}He cryostat and in the dilution cryostat, the pressure was changed at room temperature by simply turning the screws. This makes the measurement of one pressure quite long because of the cooling and heating process which takes some time. When the pressure is changed inner strains in the cell appear and the relaxation process will take some time (one hour to one night, depending on the pressure). Either the piston can be blocked a little bit or the gasket deformation is not instantaneous. After a heating

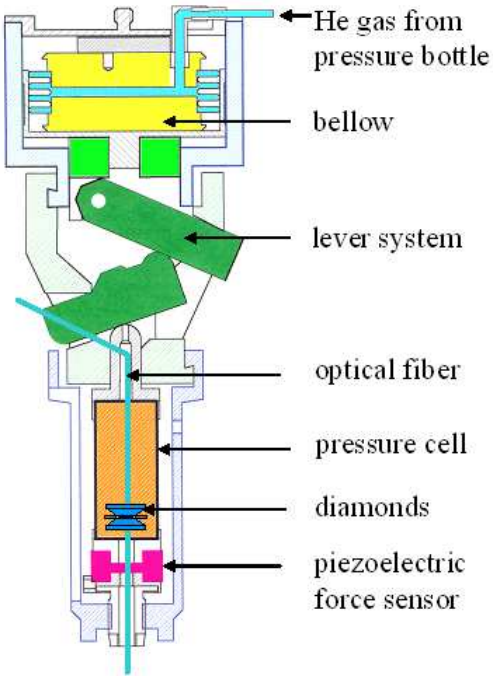

Fig. 3.8 : Scheme of the in-situ pressure tuning system in the ^{4}He cryostat [83].

and cooling process the pressure can have changed without touching the cell. The second method is described in the next paragraph.

3.4.6 In-situ pressure tuning

The ^{4}He cryostat contains a system to change pressure in-situ (see figure 3.8). For a detailed description see reference [83]. No heating and cooling is necessary to change the pressure which has an enormous advantage regarding the measurement time. Pressure is applied and changed with a bellow. He under pressure from a bottle is lead into the bellow in the cryostat. A lever system multiplies the force by a factor four and pushes the mobile piston in the pressure cell. Heating during the measurement can heat the gas-liquid mixture in the bellow which increases the pressure in the bellow. Since the pressure in the bellow and in the cell are not linearly coupled, this is usually in a range where it does not affect or change the pressure in the cell. We checked this by pressure measurements before and after the measurement. The pressure can be varied in very small steps limited basically by the resolution of the spectrometer. Steps of 0.03 GPa are possible. Sometimes the piston is blocked in its guide in the cell when the pressure in the bellow is increased. This results in uncontrollable high pressure steps when it suddenly moves again. Because this happened during the specific heat measurement series at low pressure the measured pressures were 0.3 GPa, 0.8 GPa, 1.1 GPa, 1.3 GPa. For higher pressures we didn't have this problem and could achieve smaller pressure steps.

3.5 Cooling process

3.5.1 ^{3}He cryostat

The measurements down to 450 mK were made in a ^{3}He cryostat. Here I will briefly describe its functioning. For a detailed description see for example reference [2]. As insulation between working temperature inside the cryostat and room temperature we find several layers. The dewar, also called outer vacuum chamber, is evacuated in order to diminish heat transport by diffusion of gases. Against heat transport via radiation, it is filled with about 40 layers of vacuum super insulation foil. First liquid nitrogen is filled into the dewar bringing the magnet and the dewar to 77 K. All the parts of the cryostat, where gases or liquids will circulate, and the calorimeter (inner vacuum chamber) are cleaned by pumping. After some hours or better one night the nitrogen is exchanged by liquid ^{4}He with a temperature of 4.2 K. Into this He bath, the cryostat itself with the inner vacuum chamber, filled with some mbar of He as exchange gas, is lowered from the top. It is connected to the top by several tubes for thermometer cables, measurement cables, optical fibers and ^{3}He and ^{4}He circulation. These tubes are made out of stainless steel which has a low heat conductance. Here as well we find shielding against heat radiation from the top at several levels. As soon as the cryostat is at 4 K, the inner vacuum chamber is pumped ($10^{-5} - 10^{-6}$ mbar) in order to bring out the exchange gas and to insulate the cool spots from the He bath. From the top to the bottom there is first the so called 1 K pot. It is connected via an impedance to the ^{4}He bath. Through this capillary the liquid ^{4}He gets into the 1 K pot on which we pump. This lowering of the pressure leads to a lowering of the boiling temperature to about 1.2 K. The same principle is used for the ^{3}He circuit. However the ^{3}He is injected from the reservoir at room temperature and cools on the way down in the cryostat. The ^{3}He inlet capillary is thermally connected to the 1 K pot where the gas condenses. Afterwards it flows into the ^{3}He pot and special pumps which are included into the closed ^{3}He circuit lower the pressure as well. The achieved temperature can reach down to 300 mK, but in the cryostat we used, the minimum temperature was $\sim$ 450 mK. The pressure cell is thermally connected to the ^{3}He pot. The temperature is measured with a calibrated Cernox thermometer. It is glued to a copper band which is thermally connected to the cell. The cryostat contains a superconducting magnet producing fields up to 7.5 T. The thermometer is situated in the region of compensated magnetic field. The temperature regulation is assured by a ORPX temperature controller with a regulation heater resistance.

3.5.2 ^{4}He cryostat

The cooling in this cryostat is obtained only with liquid ^{4}He and the lowest temperatures are $\sim$ 1.4 K. The most important difference is the absence of a 1 K pot. We pump on the He bath to cool below 4.2 K. This was not always the case because the interesting

temperatures were either too small for this cryostat or higher than 4.2 K.

In this cryostat we had some experimental problems. Firstly there is a leak for superfluid ^{4}He in the inner vacuum chamber. Thus the vacuum in it is uncontrolled when we pump on the He bath and lower the temperature in the He bath below 2.17 K, the transition temperature to superfluidity. Additionally a superfluid film covers parts of the inside of the inner vacuum chamber which leads to strong temperature gradients. Secondly the heating in this cryostat is not regulated. The heating power increases linearly or exponentially with time. Hence the heating rate cannot be controlled directly and depends for example on the pressure in the bellow and in the inner vacuum chamber. Resistivity and especially specific heat measurements have to be done in thermal equilibrium. If the temperature of the cell and the thermometer are not the same, the results will be wrong. A too fast heating rate as a consequence of the missing regulation can therefore result in wrong temperatures. Depending on the inner vacuum and on the pressure over the He bath the transition temperature changed significantly. This is why we will not consider the temperature measurements executed in this cryostat as absolute and basically only look at the shape of the transition. Thirdly another difficulty arises from the pressure system which is mechanically and thermally connected to the pressure cell. When heating the cell also the He gas in the bellow is heated. Therefore some of it evaporates, expands and enhances the force on the pressure cell. Usually this was in an extent where it had no effect on the pressure in the cell. The advantage of fast and easily controllable pressure is in my opinion partly compensated by the not very reliable temperature measurement in this cryostat. If detailed measurements have to be made, a solution to these problems has to be found.

3.5.3 Dilution cryostat

Very few measurements in this work were done in a dilution cryostat. In this type of cryostat we find a 1 K pot and a mixing chamber. Instead of a circuit with pure ^{3}He a mixture of ^{3}He and ^{4}He circulates. Owing to the special properties of this mixture (see for example reference [2]) this cryostat can usually cool down to several mK. During this work, it didn't cool below 50 mK, maybe because of the optical fibres bringing heat from the top. But during specific heat measurements the cell is anyway warmed up by the laser beam so the measurement startet normally at 100 mK.

Chapter 4

Results

During this work the resistivity and specific heat of URu_2Si_2 were measured under pressure and at low temperature. The main purpose was the elaboration of a detailed phase diagram but also the investiagion of the signature of the transition at T_0 for different pressures.

In order to characterise the samples #2 and 2a (cut from the first one) some preliminary measurements were necessary. In figure 4.1 the temperature dependence of specific heat and resistivity of sample #2 around the transition at T_0, measured in a PPMS at zero pressure, is compared to the resistivity of the small sample 2a in the pressure cell setup. The resistivity curves are normalised to the value at 18 K. The difference in shape is due to the fact that the resistivity was measured in different crystal directions, i.e. more in c-direction for sample 2a in the pressure cell. According to these measurements the transition temperature in specific heat is defined as the temperature at the maximum and in resistivity as the temperature at the inflection point i.e. at the minimum of the derivative (green line). The minimum of the derivative of sample 2a is at a slightly smaller temperature (dashed green line) because of the different shape of the curve and the stronger smoothing when calculating the derivative. Throughout this work the derivatives are calculated in the same manner as this derivative.

As to the superconducting transition the characterisation consists additionally of an ac-susceptibility measurement, performed in the ^{3}He cryostat with an ac-excitation field of $B \approx 15\ \mu$T and with the frequency $f = 168$ Hz by a simple coil wound with the detection coil around the sample #2. The thermal contact is achieved with the measurement wires glued to a Copper sample holder. In figure 4.2 the transition in the real part of the susceptibility signal (green line) shows a double step feature. In the specific heat (red line, PPMS measurement of sample #2) this is not as clear but also visible: Coming from high temperatures the ac-specific heat starts to grow and the real part of the susceptibility starts to fall at ~ 1.34 K, that means that a small part of the sample undergoes the phase transition. This is exactly the temperature where the resistivity is zero (black dashed line, sample 2a in pressure cell). Most of the sample however transits at a lower

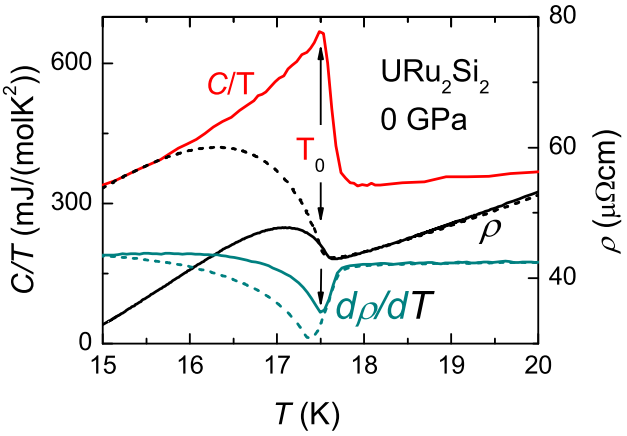

Fig. 4.1 : Temperature dependence of specific heat C/T (red line) and resistivity (black line) of URu_2Si_2 around the transition at T_0 at zero pressure for sample #2 measured in a PPMS. The dashed black line shows the resistivity of sample 2a in the uncharged pressure cell. The two resistivity curves are normalised to a value at 18 K, the difference in shape being due to different crystal directions during the measurement. The derivatives of the resistivity curves are green.

temperature $T \approx 1.15$ K. There the specific heat rises faster and the susceptibility drops faster. In this work the superconducting transition temperature in resistivity is defined as the temperature where the resistivity has dropped by half (see the construction in figure 4.2). The width of the superconducting transition is defined as the temperature difference $T_{max} - T_{min}$. In specific heat it is again defined as the temperature of the maximum.

4.1 Resistivity measurements

Figure 4.3 presents an overview of the temperature dependence of resistivity at different pressures measured in the ^{3}He cryostat. The results of the two pressure cell setups with the same sample are shown. Under pressure the transition temperature is shifted to higher temperatures and the resistivity at the transition temperature decreases. In other resistivity measurements under pressure [27], the jump in resistivity becomes significantly smaller and flatter, whereas in our measurements the anomaly stays very prominent up to high pressures. This indicates good hydrostatic conditions.

In order to compare in detail the resistivity curves at different pressures they were normalised to the minimum in resistivity as proposed by other groups (see for example [27]). In figure 4.4 are shown the curves for zero and 1.78 GPa the lowest and the highest pressure obtained with setup 1 in the ^{3}He cryostat. The curves for all other pressures lie in between. Above T_0 they overlap nicely and apart from a slight difference in the height of the jump below T_0, the anomaly has almost the same shape as a logical consequence of

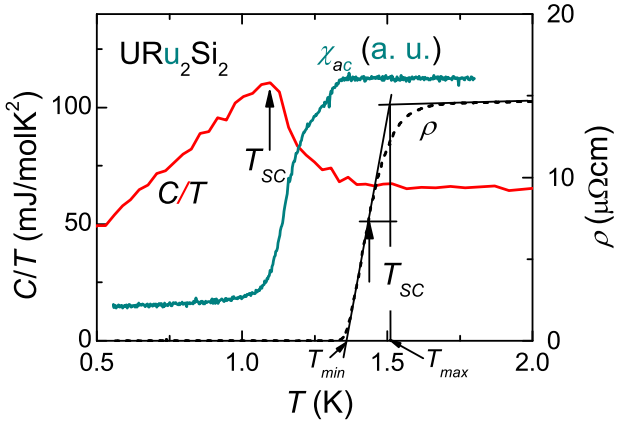

Fig. 4.2 : Temperature dependence at zero pressure of sample #2 of the specific heat C/T (red line) measured in a PPMS and of the real part of the ac-susceptibility (green line) in arbitrary units. The dashed black line shows the resistivity of sample 2a in the uncharged pressure cell.

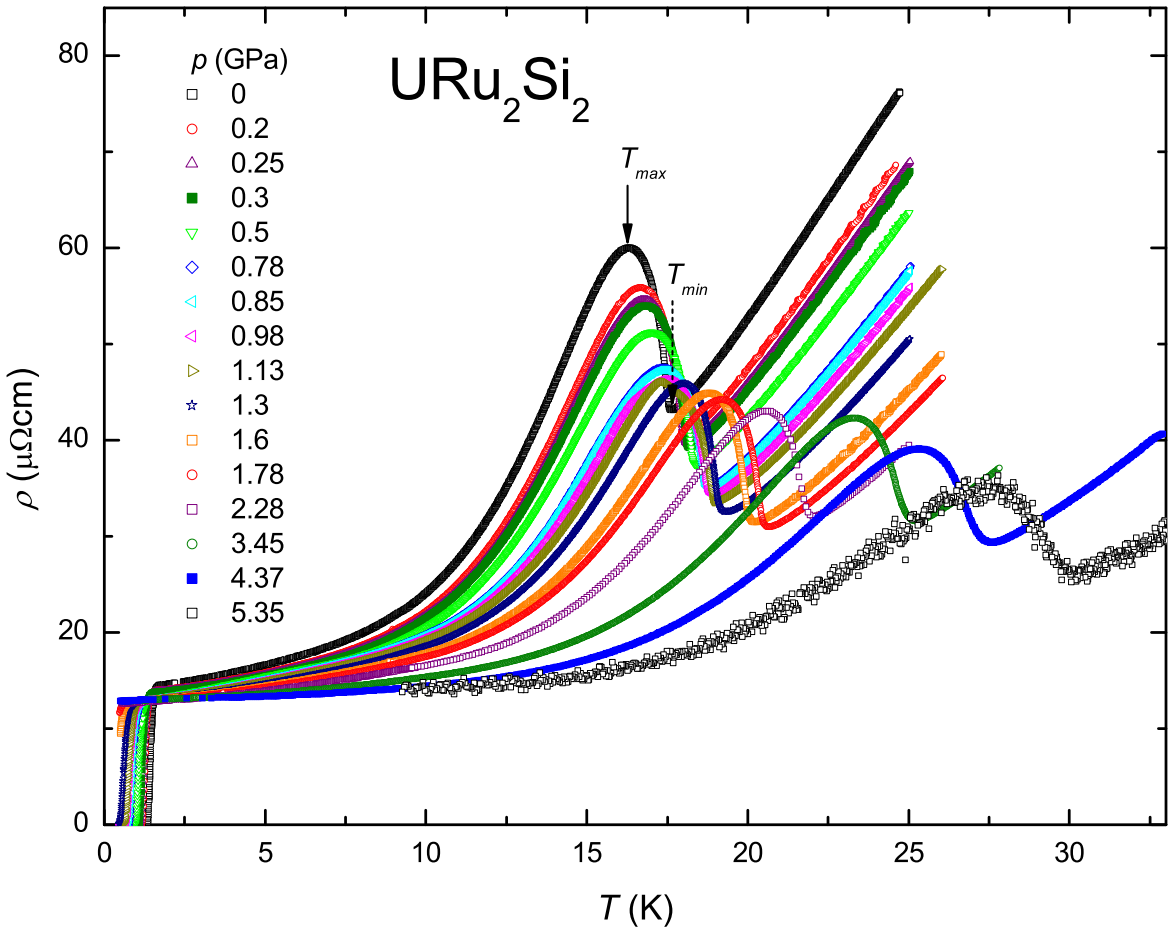

Fig. 4.3 : Temperature dependence of resistivity of URu_2Si_2 at different pressures.

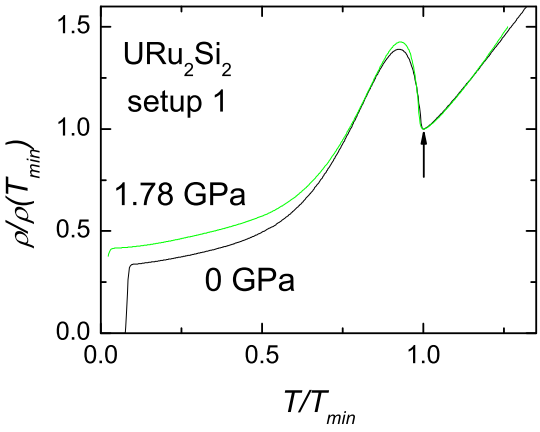

Fig. 4.4 : Normalised resistivity curves of URu_2Si_2 at 0 GPa and 1.78 GPa.

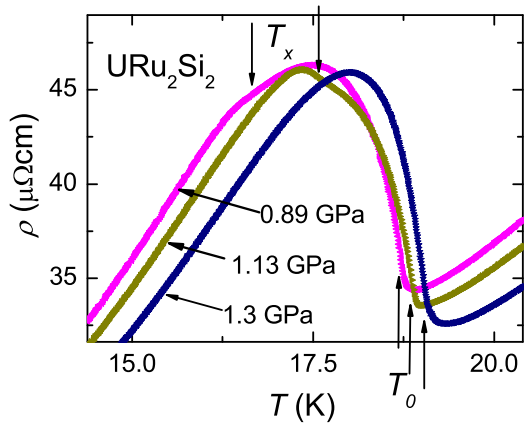

Fig. 4.5 : Temperature dependence of resistivity of URu_2Si_2 for pressures between 0.98 GPa and 1.3 GPa.

the dominance of the characteristic energy scale T_0 in this temperature region. Only at lower temperature the curves do not overlap. This means that the scattering mechanisms at low temperatures do not scale with pressure like the minimum of the resistivity. For pressures larger than 0.5 GPa, it is also not possible to fit the data according to equation 2.1 for an antiferromagnet with an energy gap $\rho = \rho_0 + AT^2 + bT(1+2T/\Delta)\exp(-\Delta/T)$. In contrast, the fit becomes quite good, when the exponent n of the AT^n term is another variable fit parameter. We will not enter in different possible origins of such derivatives clearly associated with the proximity to the pressure p_{c1} defined below.

4.1.1 Transition between hidden order and antiferromagnetism.

Looking closely at the curves at $p = 0.98$ GPa and 1.13 GPa in figure 4.5, not only the anomaly at T_0 but also a small second anomaly at T_x is visible. It is interpreted as

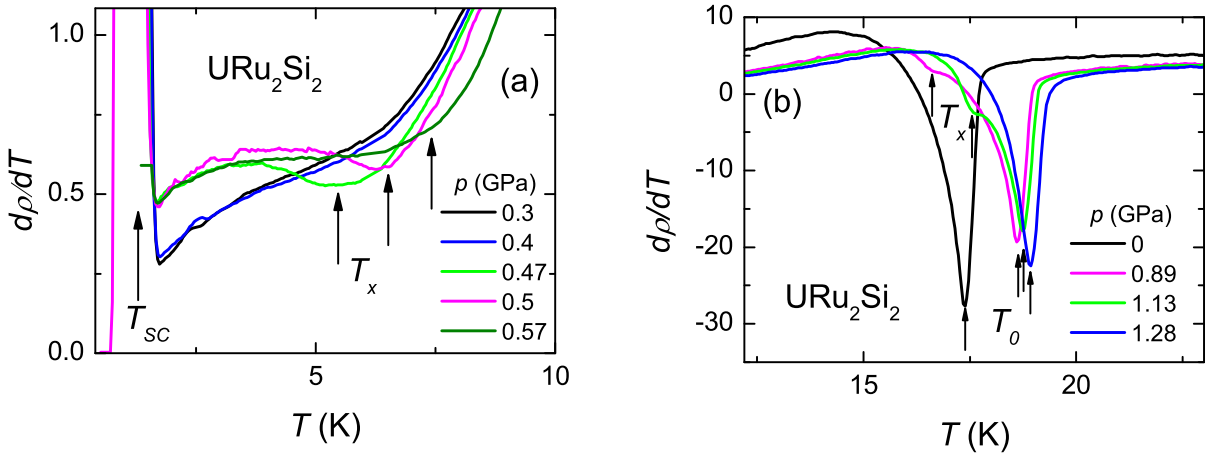

Fig. 4.6 : Temperature dependence of derivative $d\rho/dT$ of URu_2Si_2 for different pressures. The second anomaly emerges for pressures larger than 0.4 GPa. At 1.3 GPa only one anomaly is left.

the transition between the hidden order phase and the large moment antiferromagnetism and it has been observed for all pressures between 0.47 GPa and 1.25 GPa. With increasing pressure the transition temperature shifts to higher temperatures and becomes narrower and more remarkable. At low pressure the transition temperature could only be determined by taking the derivative $d\rho/dT$ and comparing directly the curves. In figure 4.6 the temperature dependence of resistivity derivatives at different pressures is presented. At 0.3 GPa and 0.4 GPa the behaviour is quite similar and then very abruptly at $p_{c1} = 0.47$ GPa the second anomaly emerges and shifts very sensitively in temperature with increasing pressure (see figure 4.6a). At higher pressures (see figure 4.6b) the second anomaly approaches the sharp minimum in the derivative at T_0 which moves much slower to higher temperature with pressure. At 1.3 GPa only one transition is left. Note that in the figure 4.6a) the y-scale is stretched in comparison to the figure on the right side. As one can see, the anomaly at T_x is very small just above the critical pressure p_{c1}. The presented curves in figure 4.6b) are the derivations of the resistivity curves in figure 4.5.

4.1.2 Superconducting transition

The superconducting transition temperature decreases for increasing pressure. The temperature dependence of the resistivity close to the superconducting transition at several pressures is presented in figure 4.7. The highest pressure where we observed the transition is 1.78 GPa. In this figure only a small part of the transition is visible, but for a smaller current the resistivity dropped to $\sim 40\%$ at the lowest temperature in the ^{3}He cryostat. Surprisingly the transition temperature depends quite strongly on the injected measurement current (see figure 4.8a). With decreasing current the transition temperature rises with an increasing slope. For small currents the two step feature seen in the susceptibility and the specific heat is recovered. This current dependence is not fully

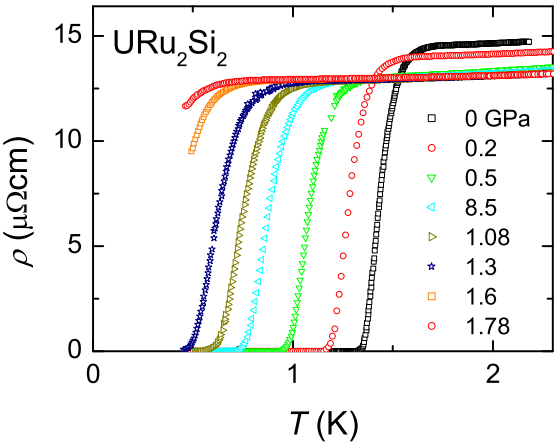

Fig. 4.7 : Temperature dependence of the superconducting transition in resistivity of URu_2Si_2 for several pressures up to 1.78 GPa.

understood but might be explained as follows: If we assume the presence of inner strains and inhomogeneities in the sample, there will be a distribution of critical temperatures T_{SC} and inhomogeneous superconductivity (along paths or the surface) is possible. For a very tiny current one superconducting path is enough to see a zero resistivity. So as the temperature is lowered the path with the highest T_{SC} will make the resistivity drop. When the current is increased the critical current density can be reached for this path and it stays in the normal state down to a lower temperature where a larger part of the sample becomes superconducting. Thus it is imaginable that the transition temperature decreases with an increasing current. If the distribution of T_{SC} is Gauss-like, then the transition temperature seen in resistivity drops first faster because the number of accessible paths grows slowly and then it will decrease slower because the number of accessible paths grows faster. For our highest currents a saturation is found because we are very far from the real critical current [85]. When plotting the transition temperature $T_{SC}(I) - T_{SC}(100\ \mu\text{A})$ against the current for different pressures like in figure 4.8b), it is evident that this behaviour does not depend on pressure.

Upper critical field

The magnetic field was applied along the symmetry axis of the pressure cell. This was unfortunately a direction with a small response of the system that means a small angle to the a-axis. The highest field $\mu_0 H = 7.5$ T almost did not affect the transition temperature T_0. The superconducting transition temperature however was suppressed by field. In figure 4.9 at a pressure of 0.78 GPa the transition could be observed up to a field of 3 T. The measurement current was chosen to 10 μA, low enough to see the transition at a high temperature but high enough to avoid too much noise. The magnetoresistance is quadratic in field as expected. Figure 4.10 shows the critical field $\mu_0 H_{c_2}/T_{SC}$ for different

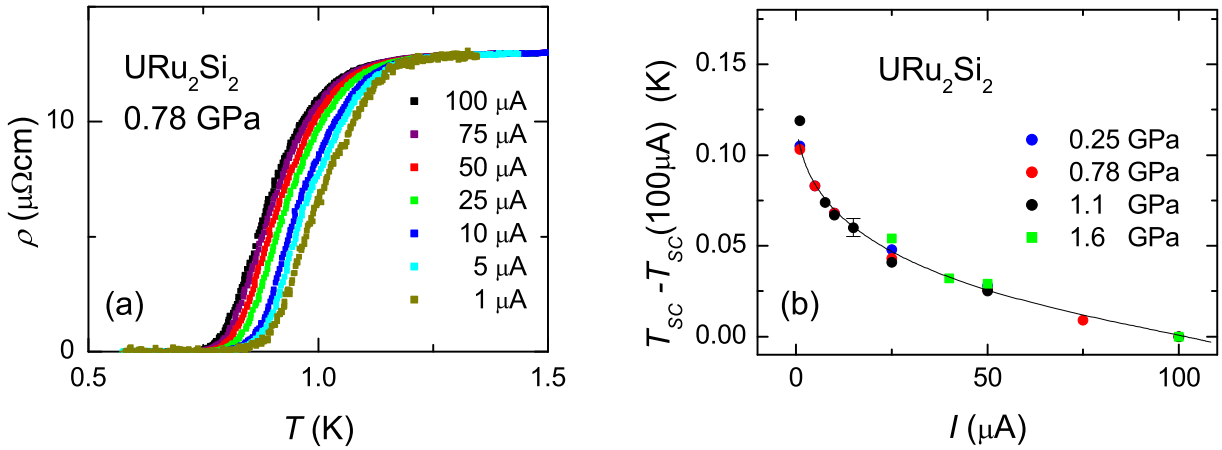

Fig. 4.8 : a) Temperature dependence of resistivity of URu_2Si_2 at 0.78 GPa for different measurement currents. b) Current dependence of superconducting transition temperature $T_{SC} - T_{SC}(100\mu A)$ for different pressures in URu_2Si_2. The error is determined from the uncertainty in the graphical determination of the transition temperature. The line is a guide to the eye.

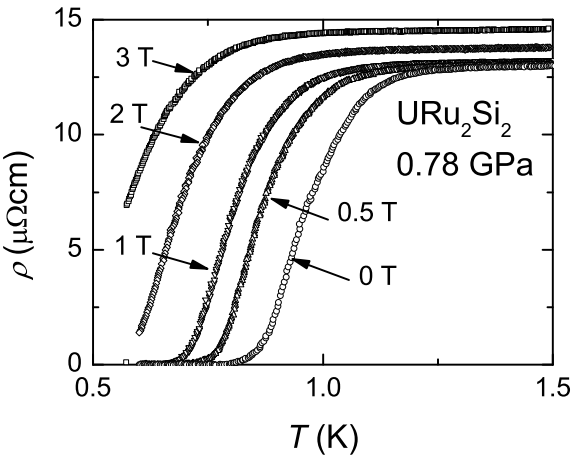

Fig. 4.9 : Temperature dependence of resistivity of URu_2Si_2 for different magnetic fields at 0.78GPa.

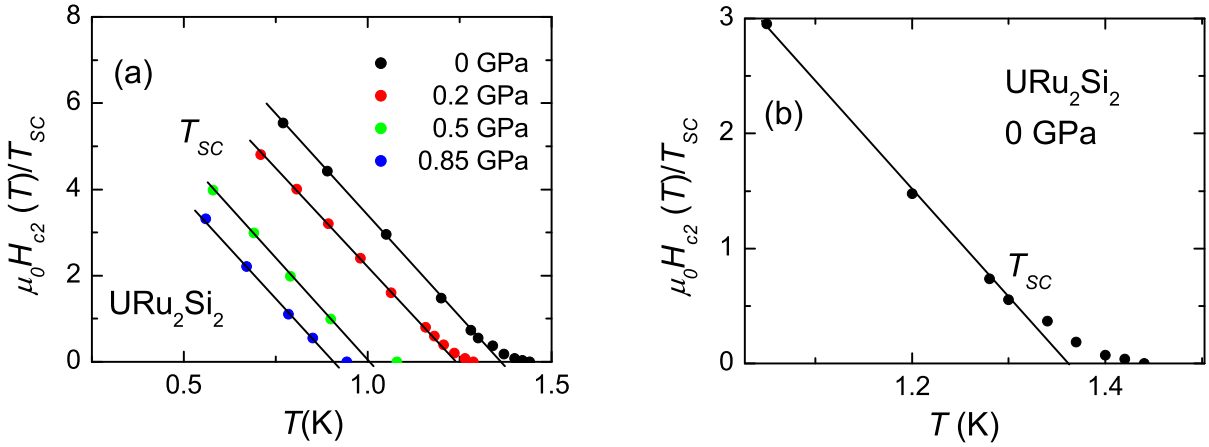

Fig. 4.10 : a) The critical field $\mu_0 H_{c_2}/T_{SC}$ of URu_2Si_2 for different pressures. Measurement current was 100 μA for all pressures except from 0.85 GPa where it was 10 μA . b) Zoom of zero pressure curve which shows upward curvature. Lines are linear fits to data for $\mu_0 H_{c_2} > 1$ T.

pressures. It was only determined via temperature sweeps. The unusual upward curvature for small fields known from previous results is found at all pressures (see figure 4.10b) [50]. Near T_{SC} we expect that T_{SC} is principally given by the orbital limit. Then the slope is given as $\frac{\partial \mu_0 H_{c_2}}{\partial T}\frac{1}{T_{SC}} \propto m^{*2}$ (see equation 1.12). From $\mu_0 H_{c_2}$ measurements the slope of the linear fits disregarding the low field data is independent of pressure. The effective mass therefore would be independent of pressure.

4.2 Specific heat measurements

A comparison of the specific heat measurement in the PPMS at ambient pressure and the signal of the ac-method at 0.3 GPa, which was the smallest pressure measured with this setup is shown in figure 4.11. The overall temperature dependence is different because the background is not subtracted in the ac-specific heat, but the shape of the anomaly is quite similar.

In the following figures the value of C/T is normalised to the value at the minimum and the absolute temperature is scaled as well for the following reasons: The transition temperature during this series of measurements was always too high ($\sim$ 0.6 K) in comparison to the resistivity measurements at the corresponding pressures probably due to temperature gradients between the sample and the thermometer. Additionally it changed depending on experimental parameters like the pressure in the inner vacuum chamber. These experimental problems have been described in paragraph 3.5.2. Nevertheless the curves at constant pressure with different experimental parameters matched nicely upon scaling the temperature for example to the temperature of the maximum of the transition. This is the reason why the measured temperature T_{mes} is normalised so that the maximum in specific heat T_{Cmax} coincides with the transition temperature T_0 from resis-

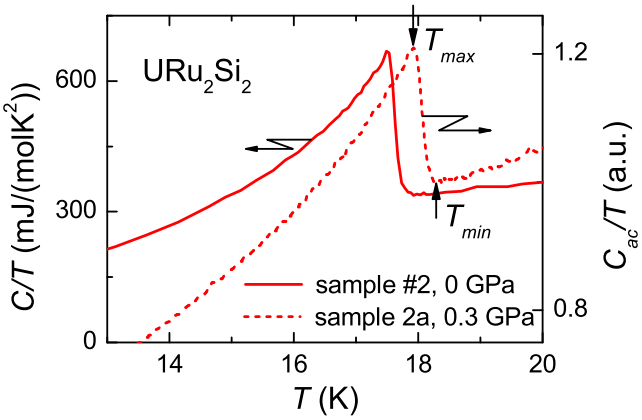

Fig. 4.11 : Temperature dependence of specific heat C/T of URu_2Si_2 measured with two different methods: ac-calorimetry under pressure at 0.3 GPa and relaxation method at ambient pressure in a PPMS. The background has not been substracted from the ac-specific heat data.

tivity measurement at the corresponding pressure: $T_{norm} = T_{mes}\frac{T_0}{T_{Cmax}}$. Doing so, a direct comparison of the shape of the transition in resistivity and specific heat is possible.

Figure 4.12 shows the ac-specific heat C_{ac}/T for different pressures. At 0.3 GPa (black curve) the transition at T_0 is very sharp and steep and its shape does not change until 1.3 GPa. This demonstrates again that our pressure conditions are excellent. The second transition which is interpreted as the transition between hidden order and antiferromagnetism is seen at 0.8 GPa and shifts to higher temperatures for 1.1 GPa and 1.3 GPa. It is very broad but becomes narrower and higher with increasing pressure. The results of specific heat measurements at higher pressures will be presented later and directly compared to the resistivity curves.

4.2.1 Superconducting transition

The specific heat at low temperature has been measured in the ^{3}He cryostat (0.1 GPa, 0.13 GPa, 0.27 GPa) and in the dilution cryostat (0.5 GPa and 0.6 GPa). A careful smooth of the temperature dependence of C_{ac}/T is shown in figure 4.13a). The transition temperature can be determined from these curves but it is much clearer in the phase of the signal (see figure 4.13b), which is the phase shift between the ac-heating and the tension of the thermocouple. For 0.5 GPa and 0.6 GPa no anomaly is visible down to the lowest temperatures of ~ 100 mK. The results shown here for different pressures are from similar heating power so that the error, originating from the average temperature elevation of the sample in comparison to the thermometer, is approximately the same (see paragraph 3.3).

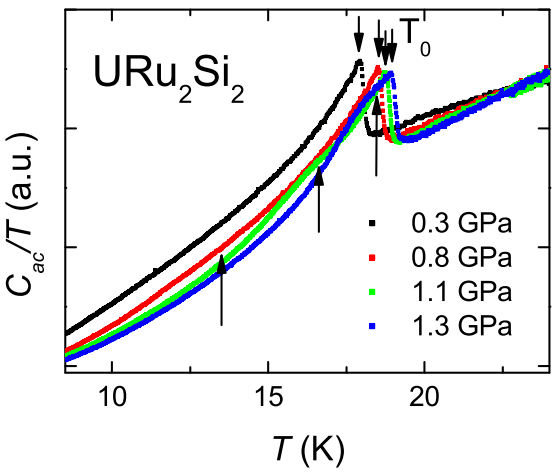

Fig. 4.12 : Temperature dependence of specific heat C_{ac}/T of URu_2Si_2 for different pressures. The temperature scale is normalised so that the maximum of the specific heat coincides with the transition temperature at the corresponding pressure according to the resistivity measurements.

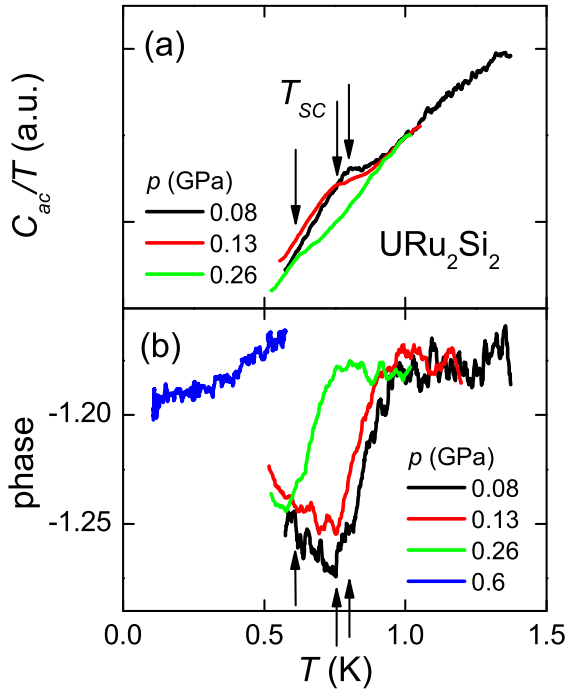

Fig. 4.13 : Temperature dependence of specific heat C_{ac}/T (a) of URu_2Si_2 and phase (b) of the ac-signal for pressures between 0.08 GPa and 0.6 GPa.

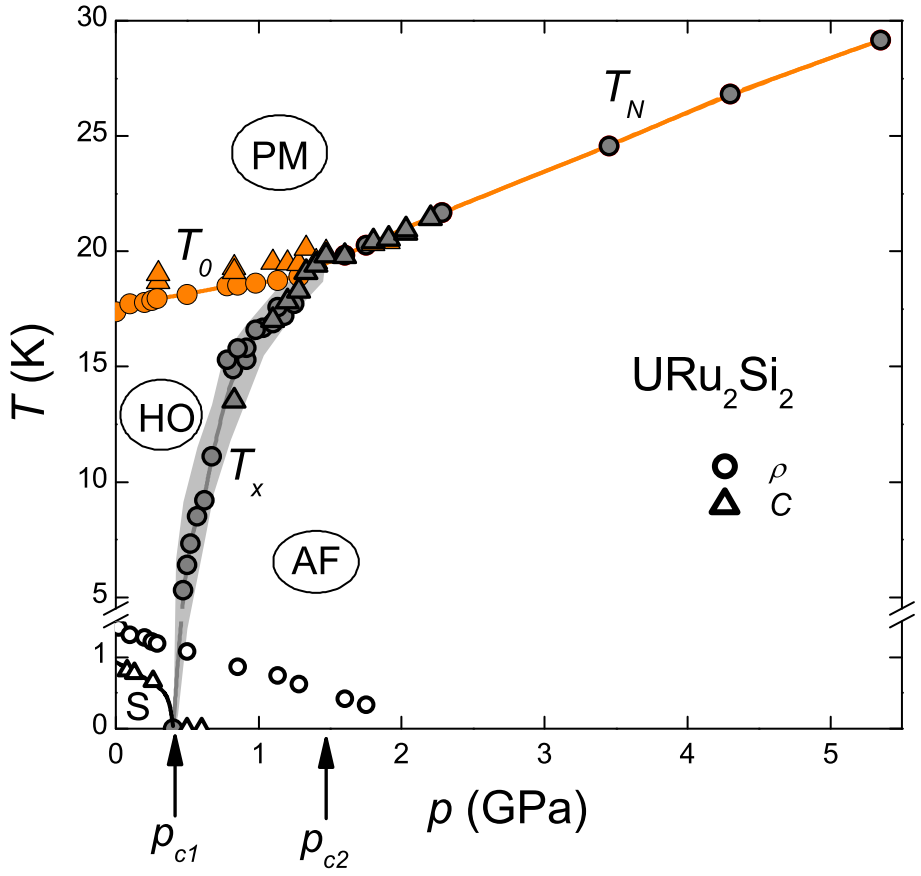

Fig. 4.14 : Pressure-temperature phase diagram of URu_2Si_2 from resistivity (circles) and specific heat (triangles) measurements. Lines are guides to the eye. The error in pressure is smaller than the symbols. The width of the transition at T_x is given approximately by the grey shadow.

4.3 Discussion

4.3.1 Pressure-temperature phase diagram

The pressure-temperature phase diagram obtained from both resistivity (circles) and specific heat (triangles) measurements is presented in figure 4.14. It is separated into four regions corresponding to four different phases. For the transition $T_0(p)$ the data from resistivity measurement in the ^{4}He cryostat are not included due to the problems of the temperature gradients in the setup. The points obtained from measurements in the ^{3}He cryostat are more precise. The error bars on the pressure are smaller than the symbols. As mentioned the transition temperatures from specific heat are too high, thus there is a large error on these points. The transition temperature rises first slowly with a slope of ~ 1.01 K/GPa and then for $p > 1.4$ GPa faster with a slope of ~ 2.61 K/GPa. This is consistent with previous measurements (see for example [28, 29, 71]). The transition line

between hidden order and antiferromagnetism $T_x(p)$ is observed in both measurement methods for the first time. It emerges at $p_{c1} \approx 0.47$ GPa and joins the other line at $p_{c2} \approx 1.4$ GPa. Just above the first pressure where the transition appears the width can be estimated to 4 K. It is shown in the phase diagram as a grey shadow. The error can be estimated from the dispersion of the values for the transition temperatures to ± 0.75 K.

Let us compare this phase diagram to the one by Amitsuka *et al.* (see figure 4.15 [39]) established from their recent neutron diffraction studies made on a small high quality single crystal of URu_2Si_2 which has therefore a smaller distribution of inner constrains. In their data, the integrated magnetic Bragg scattering intensity at $Q = (1, 0, 0)$ increases step-like at the critical pressure of the transition to large moment antiferromagnetism for a certain temperature in contrast to the continuous increase in their previous measurements [23]. That means that the pressure region where the AF-volume increases is much smaller ($\Delta p \sim 0.1$ GPa) than in NMR measurements by Matsuda *et al.* [66] or the first measurement by Amitsuka *et al.* [23]($\Delta p \approx 0.7$ GPa). The high pressure saturated value of the magnetic moment at low temperature stays however the same as before $\mu = 0.4\ \mu_B$. In their pressure-temperature phase diagram the boundary line between hidden order and antiferromagnetism emerges very steeply at a high pressure of $p \approx 0.7$ GPa. This is ~ 0.2 GPa higher than the critical pressure p_{c1} from our measurements and the higher steepness clearly points towards a first order transition line. Apart from this, the phase diagrams are quite similar and the transition lines coincide nicely. Very recent neutron scattering measurements with different pressure transmitting elements indicate that p_{c1} is shifted to lower pressure when the hydrostatic conditions are improved [86].

With the determination of the pressure dependence of the critical temperatures T_0, T_x and T_N and the concomitant measurement of the thermal expansion and the specific heat, it is possible to evaluate the consistency with the thermodynamic relations by Ehrenfest and Clapeyron for a respectively second order and first order transition. In Ehrenfest equation at a second order phase transition the change of the thermal dilatation coefficient $\Delta\alpha_v$, the jump in specific heat ΔC and the slope of the transition line in the pressure-temperature phase diagram are linked as

$$\frac{dT_c}{dp} = \frac{3\Delta\alpha_v v T_c}{\Delta C} \tag{4.1}$$

with the molar volume $v = 51$ cm^{3}mol^{-1} for URu_2Si_2 at $T = 4$ K and ambient pressure. At zero pressure deVisser *et al.* find for the thermal dilatation coefficient $\alpha_v = \frac{1}{3}(2\alpha_a + \alpha_c)$ at the transition to hidden order a jump of $\Delta\alpha = 3 \cdot 10^{-6}$ K^{-1} measured with capacitive method [67]. The measurements under pressure have been carried out by Motoyama *et al.* [24] with a resistive method and from their data (see figure 2.11) we find at zero pressure a value of $\Delta\alpha_v = 2 \cdot 10^{-6}$ K^{-1}. This method is less accurate and therefore we set the error bar to $\pm 1 \cdot 10^{-6}$ K^{-1}. With $\Delta C = 5.6$ Jmol^{-1}K^{-1} from our PPMS measurement and $T_0 = 17.5$ K we obtain $\frac{dT_0}{dp} = 0.96$ K/GPa in good agreement with our measured value of $\frac{dT_0}{dp} = 1.01$ K/GPa. To point out the contribution of the transition of T_x to the specific

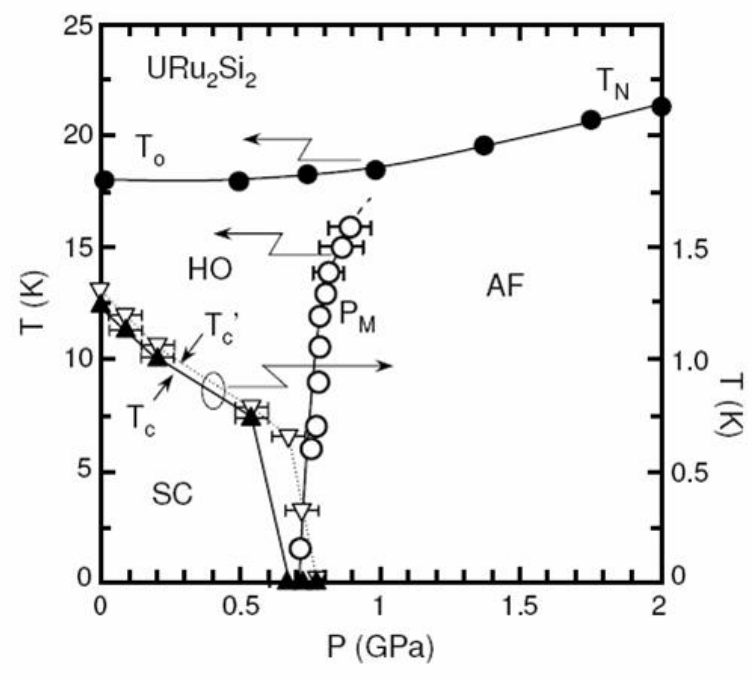

Fig. 4.15 : Pressure-temperature phase diagram of URu_2Si_2 by Amitsuka *et al.* [39]. The phase boundary line between hidden order and antiferromagnetic phase is determined from neutron diffraction data (open circles). The transition temperatures T_0 and T_N (closed) are obtained from electrical resistivity measurements with a different single crystal. Open and closed triangles represent the superconducting transition temperature T_c from susceptibility measurements on the same single crystal with two different definitions of the transition temperature. Lines are guides to the eye.

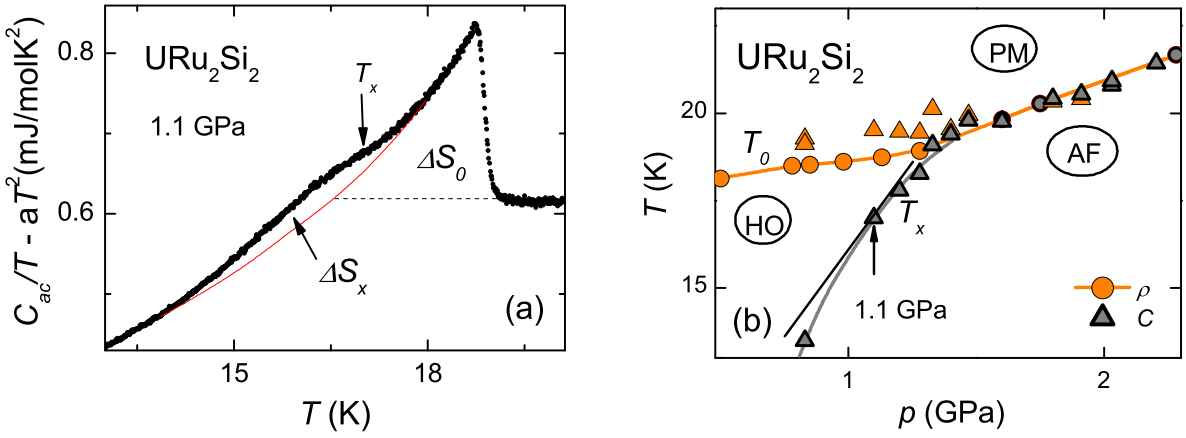

Fig. 4.16 : a) Electronic contribution of the specific heat $C_{ac}/T - aT^2$ for $p = 1.1$ GPa. The phononic contribution (determined from a $C/T = \gamma + aT^2$ fit for $T_{min} < T < T_{min} + 5$ K) has been subtracted. The red line is an approximate curve without transition with the same shape as the low pressure curves so that the contribution of the transition at T_x can be seen very clearly. b) Zoom on pressure phase diagram. The black straight line has a slope of 10 K/GPa. Lines are guides to the eye.

heat, figure 4.16a) shows the electronic contribution of the specific heat $C_{ac}/T - \beta T^2$ at $p = 1.1$ GPa. In order to determine the phonon contribution we made a $C/T = \gamma + \beta T^2$ fit for $T_{min} < T < T_{min} + 5$ K and substracted the term βT^2 from our data. One sees that the suspected first order transition at T_x does not correspond at all to the textbook figure of jump of entropy at a first order transition but to a broad signal. The reason for this might be fundamental, i.e. the transition at T_x is only weakly of first order on top of a regime with strong fluctuations, or it might be linked to the large sensitivity of the T_x line to pressure and pressure gradients. For a first order phase transition we have to apply the Clapeyron relation:

$$\frac{dT_c}{dp} = \frac{\Delta V}{\Delta S} \tag{4.2}$$

where ΔV is the volume change at the transition and ΔS is the change of entropy. From the ac-specific heat measurement, as the absolute value of C_{ac}/T under pressure is not known, we only compare the entropy of the two transitions determined in figure 4.16. With $\frac{\Delta S_0}{\Delta S_x} \approx 1.6$ and $\frac{\Delta V_x}{\Delta V_0} \approx 10$ (from the measurements by Motoyama *et al.*) the slope of the transition line $T_x(p)$ is expected to have a 16 times higher slope than the line $T_0(p)$. In figure 4.16b) is shown a zoom of the phase diagram. The straight line in this figure has a slope of 10 KGPa^{-1} which is ten times higher than the slope of $T_0(p)$. It represents nicely the slope of the specific heat data. The agreement with the calculated value is not very bad in comparison with the very inaccurate determination of ΔV.

In our phase diagram the borderline between hidden order and antiferromagnetism $T_x(p)$ seems to join the transition line $T_0(p)$. Of course this issue cannot be clarified definitively with discontinuous steps in pressure, but our measurements with quite small steps point towards two separated regions on the pressure-temperature phase diagram. In the phase diagram in figure 4.15 this is not as clear. Besides the two lines touch exactly at the pressure where the transition line at $T_0(p)$ exhibits the kink.

For the calculation of the phase diagram in Ginzburg-Landau framework according to equation 2.4 we can ascribe two order parameters to respectively the hidden order phase and the antiferromagnetic phase. In case of two order parameters that are homogeneous all over the sample, our phase diagram corresponds to the scenario $\gamma = 0$ (see the left panel of figure 2.12 [72]). That means that no linear coupling terms between the two order parameters in the Landau free energy functional exist. In this case the order parameters can break different symmetries. This is contrary to the phase diagram proposed by Bourdarot *et al.* [72] where the transition line between hidden order and antiferromagnetism ends in a critical point.

What we can learn about their nature from the signature of the transitions in resistivity and ac-calorimetry under pressure will be described in the next chapter.

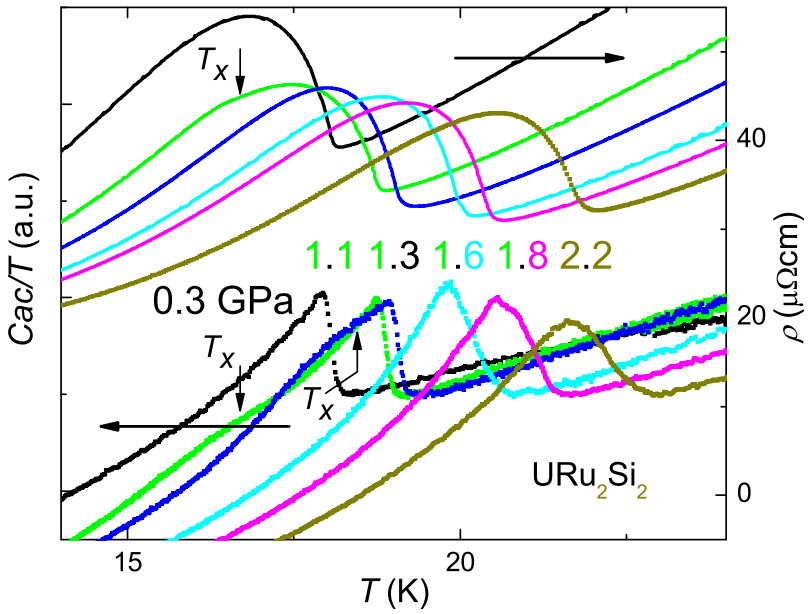

Fig. 4.17 : Temperature dependence of specific heat C_{ac}/T in comparison to resistivity in URu_2Si_2 for different pressures. The temperature scale of the specific heat measurements is normalised so that the maximum of the specific heat coincides with the transition temperature at the corresponding pressure in the resistivity measurements. Equal pressures have equal colours.

4.3.2 Transition at T_0

As the pressure phase diagram presents two distinct regions below T_0 respectively T_N, the corresponding order parameters can break different symmetries. Their microscopic differences would probably imply changes in the signature of the transitions when applying pressure. This question will be discussed in this paragraph regarding our results. In figure 4.17 we present a detailed comparison of the signature at T_0 of the specific heat C_{ac}/T and resistivity under pressure with special emphasis on the pressure region where the two transition lines touch. The temperature scale of the specific heat measurement is scaled like above. The pressures presented in the same colour are approximately the same within the error of the pressure measurement of about ~ 0.05 GPa. As mentioned before, the qualitative shape of the resistivity curves does not change. The jump in resistivity typical for a nesting of the Fermi surface persists to all measured pressures: this means that this property of the hidden order state which implies the condensation process is also present in the antiferromagnetic phase. Nevertheless looking closely at the shape some changes can be observed (see figure 4.18). At pressures below 1.3 GPa the onset of the transition coming from high temperatures is very abruptly. This is for example expressed in the temperature difference $T_{min} - T_0$ between the minimum in resistivity and the inflection

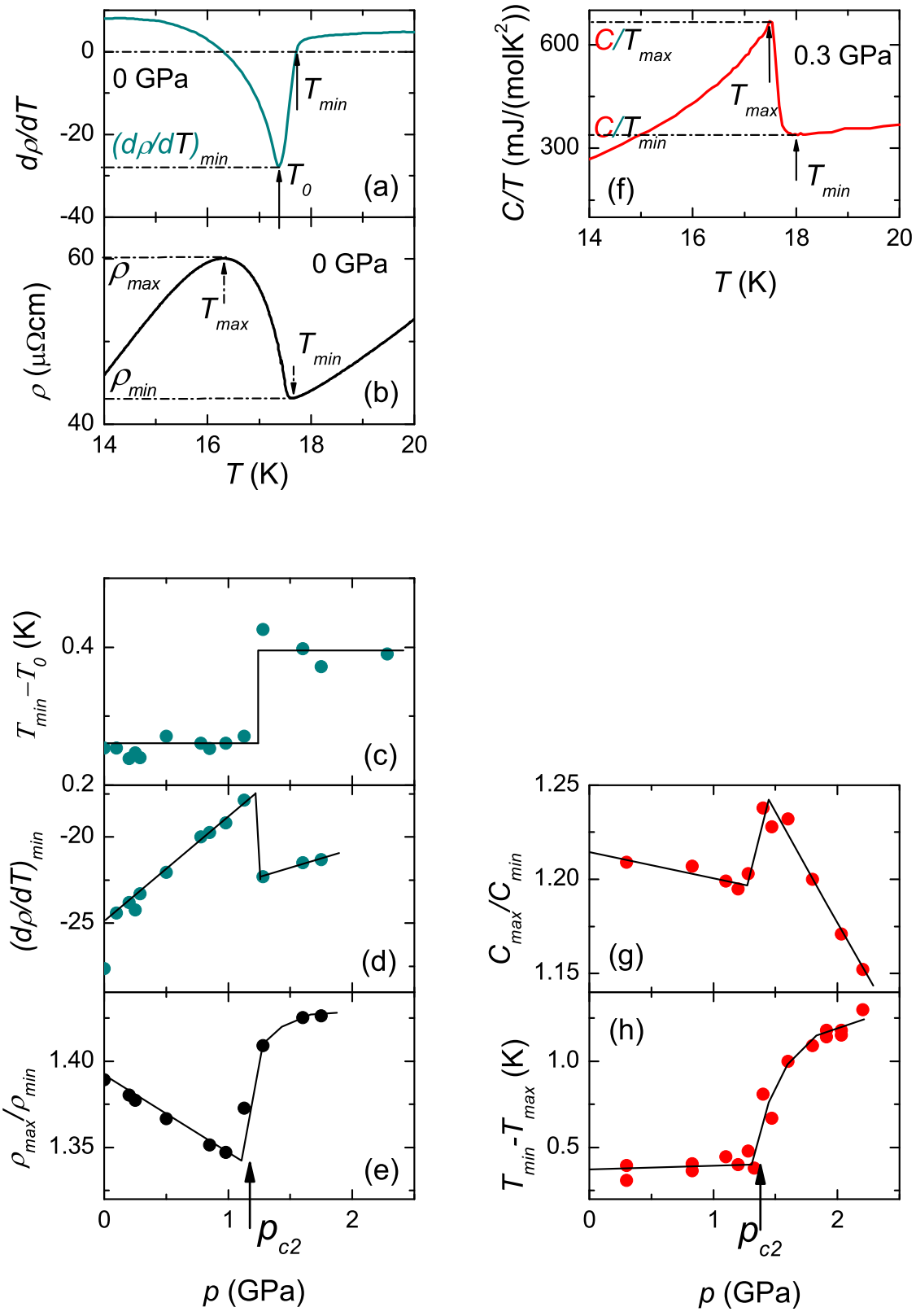

Fig. 4.18 : Pressure dependence of several parameters defined in (a, b, f) from resistivity (c, d, e) and specific heat (g, h) measurements. Lines are guides to the eye.

point, corresponding to the zero and the minimum in the derivative (see figure 4.18a). This temperature difference makes a jump at the critical pressure $p_{c2} \approx 1.3$ GPa (see figure 4.18c). At higher pressures where the transition is to the antiferromagnetic phase, the onset is consequently smoother with a lower curvature. This is also directly visible in the resistivity data (see for example figure 4.5).

The slope at the inflection point is however not smaller for higher pressures. The slope at the steepest point is given as the minimum value of the derivative $(d\rho/dT)_{min}$ (see figure 4.18a). This value can change for example with smoothing parameters. But as throughout this work the derivatives have been taken with the same numerical procedure for all resistivity curves the derivatives can be compared. The pressure dependence of the derivative's minimum value is shown in figure 4.18d). With increasing pressure the slope first decreases, i.e. the minimum value increases, and at the same critical pressure as before it suddenly jumps to a lower value.

The third parameter which indicates a change of shape of the resistivity curve is the height of the jump (see figure 4.18b). The ratio between the maximum and the minimum resistivity ρ_{max}/ρ_{min}, presented in figure 4.18(e) attenuates with pressure and jumps to a higher value at the critical pressure. The increase of this ratio already at 1.1 GPa is due to the second anomaly on top of the maximum (see the brown data in figure 4.5). The height of the jump is an indication of the part of electrons which are lost on the Fermi surface during the nesting process. At zero pressure the resistivity jumps by a factor of 1.4, that means ~ 40 % of the electrons are removed. This value first diminishes under pressure from ~ 40 % to ~ 35 % in the hidden order phase and then rises to a value of ~ 43 % in the antiferromagnetic phase.

Compared to resistivity, the specific heat changes much more obviously its shape (see figure 4.17). In analogy to the resistivity curves the ratio between the maximum and minimum specific heat $(C/T_{max})/(C/T_{min})$ versus pressure as defined in figure 4.18f) is traced in figure 4.18g). It attenuates slowly until a critical pressure $p_{c2} \approx 1.3$ GPa, where it jumps to a higher value. For increasing pressure it decreases then faster.

The width of the transition, defined as the temperature difference between the minimum and maximum $T_{min} - T_{max}$ (see figure 4.18f), is strongly enhanced at the same critical pressure p_{c2} (see figure 4.18h). Summarising, one could say that the shape of the specific heat curves is much more symmetric for pressures higher than p_{c2}. The critical pressure is a little bit higher than the one determined from resistivity measurements. In all shown parameters the change of shape of the transition at T_0 to hidden order ($p_{c2} < 1.3$ GPa) respectively antiferromagnetism ($p_{c2} > 1.3$ GPa) is distinct, even if the effect in resistivity is small, and it happens quite abruptly at a critical pressure of $p_{c2} \approx 1.3$ GPa.

Besides the quantitative description of the signature of the transition at T_0 a detailed qualitative description is necessary. Let us therefore look closer to the C_{ac}/T curves in figure 4.17. The large bump of the second anomaly at T_x comes up with pressure. At

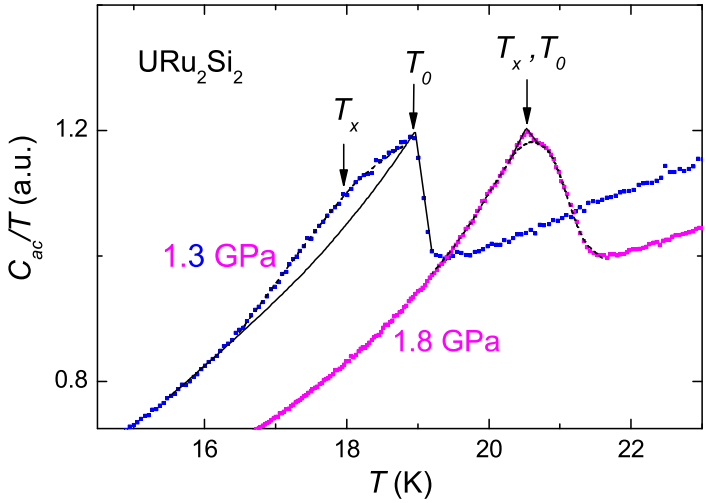

Fig. 4.19 : Pressure dependence of specific heat C_{ac}/T in URu_2Si_2 for 1.3 GPa (pink) and 1.8 GPa (blue). Lines are guides to the eye.

1.1 GPa (green data) it is visible in both resistivity and specific heat and its position coincides well. At 1.3 GPa in resistivity only one transition is left, whereas in specific heat both transitions are discernible. The contributions from the two different anomalies are estimated as presented by the black lines in figure 4.19. The contribution of the anomaly at T_x (dashed line) is relatively small and broad for 1.3 GPa. The contribution of the sharp step-like transition at T_0 (solid line) has not changed its shape in comparison to lower pressures. As T_0 increases slower with pressure than T_x, for higher pressures the round bump at T_x shifts up further in temperature and the anomalies superpose. This is the pressure region where the two get close. With increasing pressure in this region, the intensity of the sharp anomly is attenuated whereas the intensity of the round anomaly increases. At 1.8 GPa the transition at T_0 is dominated by it i.e. the contribution of the transition at T_0 is only left as a small peak on top of the large round anomaly (see fig 4.19). For all higher pressures, only the round anomaly is observed. From the specific heat data I suppose that always $T_0 \geq T_x$ and that in the pressure phase diagram the transition line at T_0 ends when the borderline between hidden order and antiferromagnetism comes up and transforms into the transition line at T_N between the para- and the antiferromagnetic state.

To summarize we can say that the shape of the transition in resistivity is only slightly affected by pressure and therefore the nesting takes place at all measured pressures. If this rearrangement of the Fermi surface (due to some sort of spin density wave) is one characteristic of the hidden order, this would mean that this characteristic of the hidden order parameter is also non-zero for high pressures. But from the specific heat measurements the shape at T_N is totally different from the signature at T_0. So the transition at T_N is not a continuation of the transition at T_0.

In URu_2Si_2 itinerant (some sort of spin density wave) and local (local antiferromagnetism) properties are coupled. Probably the gap-opening is a necessary condition for magnetic ordering: When a part of the electrons is removed from the Fermi surface, the hybridisation is weakened and therefore the local character of the f-electrons becomes more important. Thus the $5f$-bandwidth gets smaller, which leads to long range magnetic order of almost localised moments. This coupling is the reason why the nesting temperature follows the ordering temperature T_N, which seems to be the extension of the line $T_x(p)$.

Dc-magnetisation measurements show a qualitatively equal behaviour for low and high pressures, but reveal a change of the temperature derivative $\frac{\partial M}{\partial T}$ in the antiferromagnetic phase. That means that the slope just below T_0 decreases by half for B and M$\|$c and increases by a factor of 15 for B and M$\|$a at $p \approx 1.7$ GPa [28] compared to the zero pressure curves.

Our measurements cannot reveal the real nature of the hidden order. New time-of-flight neutron diffraction at ambient pressure by Wiebe *et al.* shed some more light on this question. We already mentioned that two kinds of spin excitations exist in URu_2Si_2, both gapped below T_0 (see paragraph 2.1). The excitations with a wave vector $Q_0 = (1, 0, 0)$ in reciprocal space correspond to the local antiferromagnetism with propagation vector (0, 0, 1) and the second type of itinerant-like spin excitations is found at the incommensurate wave vecor $Q = (1, 0.4, 0)$ and equivalent ones. Wiebe *et al.* could show that the spectrum above T_0 is dominated by the latter itinerant-like spin excitations [87]. These spin fluctuations occupy much more of phase space than those at magnetic Bragg peaks and their gapping below T_0 can therefore account for the large entropy removal at the transition. This supports the fact that itinerant rather than local electron physics determine the transition at T_0 and the hidden order state. In recent NMR measurements no evidence for magnetic ordering at ambient pressure is found [88]. This points towards the fact that in a perfect crystal of URu_2Si_2 magnetism is not present in the hidden order phase but only emerges under pressure. Thus the order parameter of the hidden order state would be non-magnetic. The proposed theoretical models with an order parameter consisting of a magnetic dipole would then be ruled out and the possibilities left are quadrupolar [56, 57] or octupolar ordering [58], unconventional density waves [59], helicity order [60], orbital antiferromagnetism [61] or Jahn-Teller distortion [62]. It is an interesting question, how the mentioned excitations behave under pressure. Inelastic neutron scattering under pressure is definitively necessary to study for example the behaviour of the two gaps at the critical pressures and to determine the microscopic nature of the order parameters of the hidden order and the antiferromagnetic phase.

4.3.3 Low temperature behaviour

At low temperature above T_{SC} we expect a quadratic temperature behaviour of the resistivity within Fermi-liquid theory. Therefore the data are fitted according to the formula

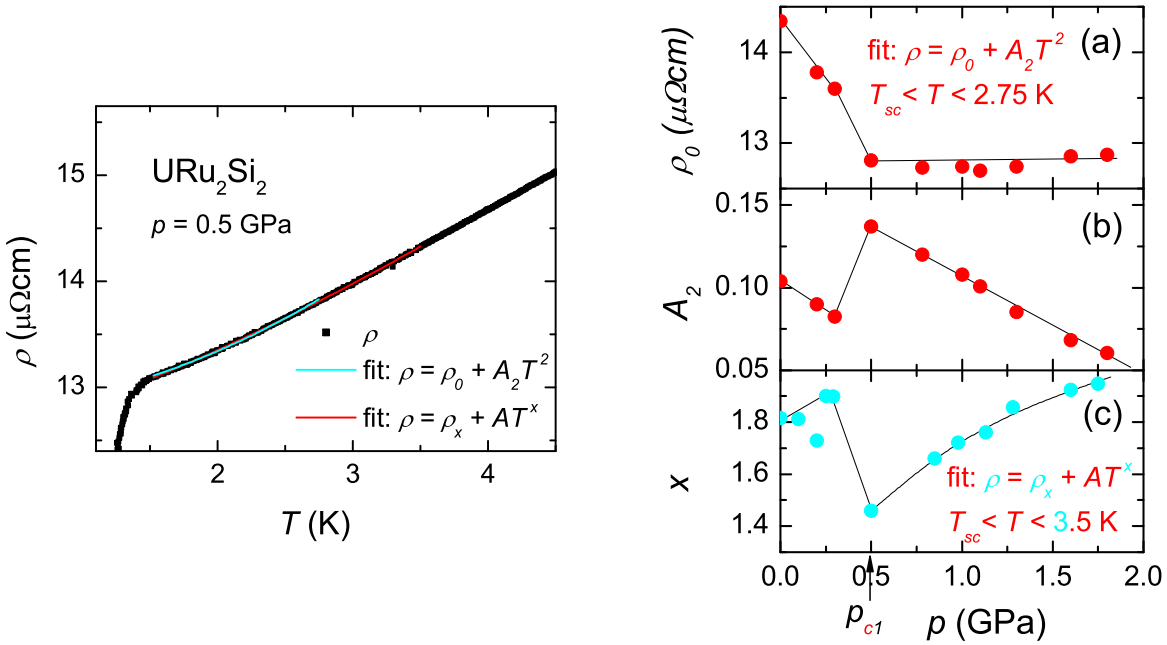

Fig. 4.20 : On the left: Low temperature fits at 0.5 GPa of the resistivity of URu_2Si_2. One the right: Pressure dependence of low temperature fit parameters. In (a) and (b) are shown the fit parameters of a $\rho = \rho_0 + AT^2$ fit for $T < 2.75$ K. In (c) is presented the exponent x of a $\rho = \rho_x + AT^x$ fit for $T < 3.5$ K. Lines are guides to the eye.

$\rho = \rho_0 + A_2T^2$ for temperatures between the superconducting transition and 2.75 K (see there fit on the left side of figure 4.20). The pressure dependence of the fit parameters ρ_0 and A_2 is presented in figure 4.20a) and b) on the right. The residual resistivity ρ_0 decreases first linearly and stays then at a constant value for pressures $p \geq 0.5$ GPa. The coefficient A_2 of the T^2 term decreases with pressure, makes a jump at $p_{c1} \approx 0.5$ GPa and continues its decline. However the T-dependence at low temperature is more likely not quadratic. If the fit is extended to a larger temperature range up to 3.5 K, only an exponent smaller than 2 is able to fit the data accurately (see the blue fit on the left side of figure 4.20). Consequently in figure 4.20(c) is presented the pressure dependence of the exponent x in a $\rho = \rho_x + AT^x$ fit. At low pressure it is close to 2, then drops to a value $< 3/2$ at 0.5 GPa. From there on it grows steadily until reaching again approximately 2 at ~ 1.8 GPa. Just above the critical pressure p_{c1} definitely a non-Fermi-liquid behaviour is found. This coincides with a first order transition at ~ 0.5 GPa where the antiferromagnetic phase emerges.

4.3.4 Superconducting transition

In figure 4.21a) is shown a zoom of the pressure phase diagram at low pressure and low temperature. In resistivity the superconducting transition temperature was determined from measurements with a current of 100 μA. In resistivity the superconductivity is seen up to $p = 1.8$ GPa deep in the antiferromagnetic phase. The result is similar as in previous

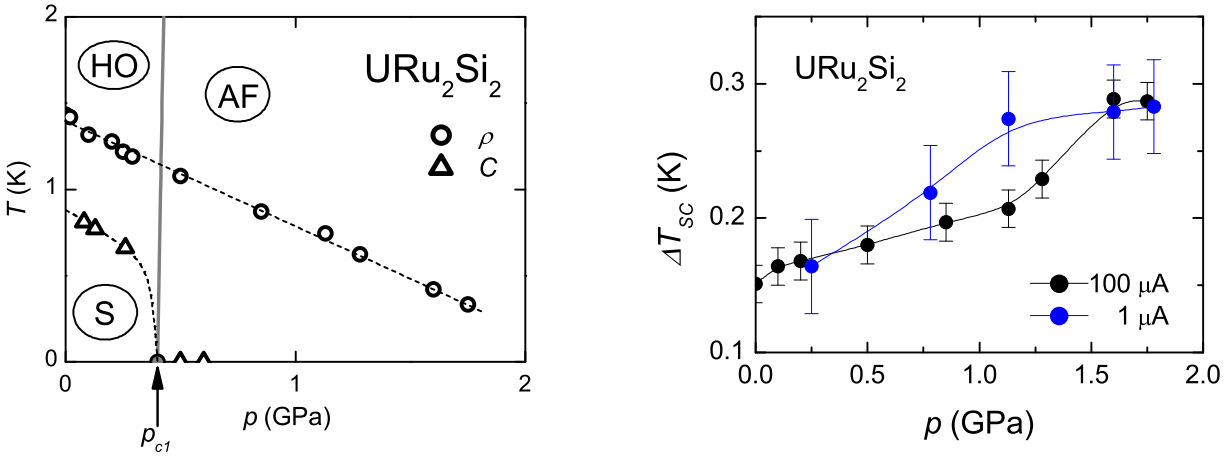

Fig. 4.21 : a) Pressure-temperature phase diagram of URu_2Si_2 at low temperature. b) Pressure dependence of width of the superconducting transition for a measurement current of 100 μA (black) and 1 μA (blue). The lines are guides to the eye.

resistivity measurements, but the highest pressure, where the transition is observed is higher than in those measurements with $p = 1.2$ GPa [27] and [29]. Tenya *et al.* claim that the superconducting phase transition disappears above 1.5 GPa from magnetization measurements [89]. In specific heat measurements in contrast, the transition is not seen at 0.5 GPa and 0.6 GPa down to 100 mK in our measurements. Specific heat is a bulk property, so that volumic superconductivity in URu_2Si_2 is assumed to be suppressed by the antiferromagnetic phase. This is consistent with the susceptibility data by Uemura *et al.* [30]. The resistivity measurement shows however that on the surface or paths through the sample a current can pass without resistance up to at least 1.8 GPa. This could be due to small inhomogeneous areas in the sample which are not antiferromagnetic at a pressure where normally antiferromagnetism dominates. Here again we could argue with inner strains causing a certain pressure distribution in the sample. It is though quite surprising that neither the width of the superconducting transition (see figure 4.21b) nor its current dependence change at the critical pressure. The same holds for the upper critical field. The unchanged slope under pressure points towards an unchanged effective mass. But as the coefficient A of the T^2 term in the low temperature fit of the resistivity curves is proportional to m^{*2} as well, one should expect that in makes a jump at the critical pressure and especially that it decays with pressure. This had been found by McElfresh *et al.* and Schmidt *et al.* who both found a continual decrease of m^* [27, 29]. But their pressure steps were much larger up to higher pressures so that they did not see the critical pressure. But looking closely at the data by McElfresh *et al.* the jump in the fit parameter A from a $\rho = \rho_0 + AT^2$ fit can even be observed.

With the suppression of superconductivity by the antiferromagnetic phase URu_2Si_2 behaves differently than other uranium heavy fermion compounds like UPd_2Al_3 for example, which orders antiferromagnetically at $T = 14$ K and becomes superconducting at $T_{SC} = 2$ K [90].

Conclusion

The results of ac-calorimetric and resistivity measurements of URu_2Si_2 under pressure up to 5.5 GPa have been presented.

The pressure-temperature phase diagram we obtained is very detailed and shows four distinct regions corresponding to four different phases. The hidden order phase, which develops below the transition temperature T_0 at ambient pressure, is seperated from a large moment antiferromagnetic phase by a first order transition line $T_x(p)$, which has been seen for the first time in resistivity and specific heat. This line emerges at a critical pressure p_{c1} and joins the transition line $T_0(p)$ at the pressure p_{c2}. The first critical pressure p_{c1} is sample dependent (for our sample $p_{c1} \approx 0.47$ GPa) whereas the second critical pressure does not vary a lot comparing different publications ($p_{c2} \approx 1.4$ GPa). The tiny pressure steps and the development of the signature of the ac-specific heat allows us to conclude that the transition line between hidden order and antiferromagnetism does not end in a critical point. As a consequence, the order parameters of the two phases can have different symmetries.

Regarding this question the signature of the transitions under pressure in resistivity and specific heat was investigated. On the one hand the results in resistivity indicate that the condensation process due to the formation of a spin density wave state is also present at high pressure. On the other hand the shape of the transition seen by ac-calorimetry changes significantly at the pressure p_{c2}. The transition temperatures are the same, so maybe the order parameter of the spin density wave is for high pressures coupled to the antiferromagnetic order parameter. Here, further microscopic measurements are necessary

Finally concerning the superconducting transition, the results from the two measurement methods show different results. In resistivity the transition temperature was visible up to 1.8 GPa and in ac-specific heat, it is not visible any more at 0.5 GPa down to 100 mK. Because specific heat is a probe for bulk properties, this means that superconductivity in URu_2Si_2 can only coexist with the hidden order state and is suppressed rapidly under pressure, when the large moment antiferromagnetic phase emerges. This behaviour is usually typical for Ce heavy fermion superconductors, where the region of coexistance between antiferromagnetism and superconductivity is narrow, whereas in U heavy fermion compounds superconductivity can coexist with magnetism over a large pressure range maybe due to the dual character of the $5f$-electrons.

Bibliography

[1] G. R. Stewart, Rev. Mod. Phys. **56** (1984)

[2] C. Enss and S. Hunklinger, Low Temperature Physics (Springer Verlag, Heidelberg, 2005)

[3] M. A. Rudermann, C. Kittel, Phys. Rev. **96**, 99 (1954)

[4] T. Kasuya *et al.*, J. Magn. Magn. Mater. **76,77** (1988)

[5] G. Zwicknagl *et al.*, Phys. Rev. B **65**, 081103 (2002)

[6] J. Kondo, Prog. Theor. Phys. **32**, 37 (1964)

[7] E. Bauer, lecture script, Wien

[8] S. Doniach, Physica B **91**, 231 (1977)

[9] N.B. Brandt, Adv. Phys. **33**, 373 (1984)

[10] J. Flouquet, Progress in Low Temperature Physics Vol. 15, W. Halperin (Elsevier, Amsterdam, 2005) p.139

[11] Q. G. Sheng *et al.*, J. Appl. phys. **75** (1994)

[12] G. Knebel *et al.*, Phys. Rev. B **65**, 024425 (2002)

[13] A. J. Millis, Phys. Rev. B, **48**, 7183 (1993)

[14] G. G. Lonzarich, Electron, M. Springford (Cambridge University Press, 1997).

[15] N. D. Mathur *et al.*, Nature **394**, 39 (1998)

[16] Spin density wave, Wikipedia

[17] E. Fawcett, Rev. Mod. Phys. **60(1)**, 209-283 (1988)

[18] E. Fawcett *et al.*, Rev. Mod. Phys. **66(1)** (1994)

[19] A. Verniere *et al.*, Physica B **206-207**, 509 (1995)

[20] A. Verniere *et al.*, J. Magn. Magn. Mater. **153**, 55 (1996)

[21] T.T.M. Palstra *et al.*, Phys. Rev. Lett. **55**, 2727 (1985)

[22] C. Broholm *et al.*, Phys. Rev. Lett. **58**, 1467 (1987)

[23] H. Amitsuka *et al.*, Phys. Rev. Lett. **83**, (1999)

[24] G. Motoyama *et al.*, Phys. Rev. Lett. **90**, 166402 (2003)

[25] A. Amato *et al.*, J. Phys. Cond. Mat. **16**, S4403 (2004)

[26] M. Yokoyama *et al.*, Phys. Rev. B **72**, 214419 (2005)

[27] M. W. McElfresh *et al.*, Phys. Rev. B **35**, 43 (1987)

[28] C. Pfleiderer *et al.*, arxiv:Cond. Mat.(2006)

[29] L. Schmidt, doctoral thesis

[30] S. Uemura *et al.*, J. Phys. Soc. Jpn. **74**, 2667 (2005)

[31] W. Schlabitz *et al.*, abstract presented at Fourth International Conference on Valency Fluctuations, Cologne 1984

[32] K. Hiebl *et al.*, J. Magn. Magn. Mater. **37**, 287 (1983)

[33] T.T.M. Palstra *et al.*, Phys. Rev. B **33**, 6527 (1986)

[34] N. Hessel Andersen, Crystalline Field and Structural Effects in f-Electron Systems, J. E. Crow, R. P. Guertin, and T. W. Mihalism (Plenum, New York, 1980), p. 373

[35] M. B. Maple *et al.*, Phys. Rev. Lett. **56**, 185 (1986)

[36] J. G. Park *et al.*, Cond. Mat. **9**, 3065 (1997)

[37] D. A. Bonn *et al.*, Phys. Rev. Lett. **61**, 1305 (1988)

[38] P. A. Sharma *et al.*, Phys. Rev. Lett. **97**, 156401 (2006)

[39] H. Amitsuka *et al.*, J. Magn. Magn. Mater. **0**, 1 (2006)

[40] T. E. Mason *et al.*, Phys. Rev. Lett. **65**, (1990)

[41] B. Fåk *et al.*, J. Magn. Magn. Mater. **154** (1996)

[42] T. Honma *et al.*, J. Phys. Soc. Jpn. **68**, 338 (1999)

[43] C. Broholm *et al.*, Phys. Rev. B **43**, 12809 (1991)

[44] C. Marcenat *et al.*, J. Magn. Magn. Mater. **76-77**, 115 (1988)

[45] G. Aeppli *et al.*, Phys. Rev. Lett. **60**, (1988)

[46] G. R. Stewart *et al.*, Phys. Rev. Lett. **52**, (1984)

[47] C. R. Wiebe *et al.*, arxiv:Cond. Mat.(2003)

[48] M.-A. Measson *et al.*, Phys. Rev. B **70**, 064516 (2004)

[49] W. K. Kwok *et al.*, Phys. Rev. B **41**, 11649 (1990)

[50] J. P. Brison *et al.*, Physika C **250**, 128 (1995)

[51] H. Ohkuni *et al.*, Pilosophical Magazine B **79**, 1045 (1999)

[52] G. J. Nieuwenhuys *et al.*, Phys. Rev. B **35**, 5260 (1987)

[53] N. Bernhoeft *et al.*, Acta Phys. Polonica B **35**, 1367 (2003)

[54] V. P. Mineev *et al.*, Phys. Rev. B **72**, 014432 (2005)

[55] Y. Okuno *et al.*, J. Phys. Soc. Jpn. **67**, 2469 (1998)

[56] P. Santini *et al.*, Phys. Rev. Lett. **73**, 1027 (1994)

[57] F. J. Ohkawa *et al.*, J. Phys.Cond. Mat. **11**, L519 (1999)

[58] A. Kiss *et al.*, Phys. Rev. B **71**, 054415 (2005)

[59] H. Ikeda *et al.*, Phys. Rev. Lett. **81**, 3723 (1998)

[60] C. M. Varma *et al.*, Phys. Rev. Lett. **96**, 036405 (2006)

[61] P. Chandra *et al.*, Physika B **312-313**, 397 (2002)

[62] T. Kasuya, J. Phys. Soc. Jpn. **66**, 3348 (1997)

[63] F. R. deBoer *et al.*, Physica B **139**, 1 (1986)

[64] K. Iki *et al.*, J. of Alloys and Compounds **181**, 71 (1992)

[65] K. Matsuda *et al.*, Phys. Rev. Lett. **87**, 087203 (2001)

[66] K. Matsuda *et al.*, J. Phys. Cond. Mat. **15**, 2363 (2003)

[67] A. deVisser *et al.*, Phys. Rev. B **34**, 8168 (1986)

[68] K. Bakker *et al.*, J. Magn. Magn. Mater. **108**, 63 (1992)

[69] J. A. Mydosh *et al.*, arxiv:Cond. Mat.(2002)

[70] N. Shah *et al.*, Phys. Rev. B **61**, 564 (2000)

[71] G. Knebel *et al.*, J. Magn. Magn. Mater. , (2006)

[72] F. Bourdarot *et al.*, Physica B **359-361**, 986 (2005)

[73] M. Nakashima *et al.*, J. Phys. Cond. Mat. **15**, S2011 (2003)

[74] K.-W. Hasselbach, doctoral thesis (1991).

[75] Demuer A *et al.*, J. Low Temp. Phys. **120**, 245 (2000)

[76] Wilhelm H and Jaccard D 2002 JPCM **14** 10683

[77] P. F. Sullivan *et al.*, Phys. Rev. Lett. **173**, 679 (1986).

[78] J.Chaussy *et al.*, J. low temp. phys. **49**, 167 (1982)

[79] E. S. Itskevich V. F. Kraidenov, Instrum. Exp. techn. **21**, 1640 (1979)

[80] G. Knebel *et al.*, J. Phys. Cond. Mat. **16**, 1 (2004)

[81] J. Tomasson *et al.*, private communications (1989)

[82] R. A. Noack and W. B. Holzapfel, High Pressure Sience and Technology, K. D. Thimmerhaus and M. S. Barber (Plenum New York, 1979)

[83] B. Salce *et al.*, Phys. Rev. Instrum. **71** (2000)

[84] H. L. Alberts, S. Afr. J. Sci. **84**, 32-34 (1988)

[85] S. Wüchner *et al.*, Solid State Comm. **85**, 355 (1993)

[86] H. Amitsuka *et al.*, conference on strongly correlated electron systems SCES, Houston (2007)

[87] C. R. Wiebe *et al.*, Nature (2007)

[88] S. Takagi *et al.*, J. Phys. Soc. Jpn. **76**, 033708 (2007)

[89] K. Tenya *et al.*, Physica B **359-361**, 1135 (2005)

[90] C. Geibel *et al.*, Zeitschrift für Physik B, Condensed Matter **84**, 1 (1991)

Ackowledgement

First of all I am very grateful to Prof. Enss who made this Diplomarbeit possible and to the whole group in Heidelberg. They made me feel welcome during our stay in Regensburg.

I thank my supervisor Jacques Flouquet who led me during this work with his great knowledge and enthusiasm.

Thanks to Georg for being there for any questions, experimental, theoretical and personal.

I am very greatful to Bernard Salce, who allowed me to use his efficient machine for my measurements.

For providing and characterising the sample and for a brief introduction into crystallography I thank Pascal Lejay.

I appreciated the work with Albin Demuer, who helped me cutting my sample with incredible exactness.

For the introduction to neutron scattering techniques I thank Frederic Bourdarot, the "pro" of URu_2Si_2.

I thank Daniel Braithwaite for the corrections of mistakes of the english language.

Without the help of the technicians in case of material problems, my experiments would have stopped for a long time. I thank them for their presence and help.

I also thank Estelle and Alain, who made the time spent in the labratory nice with a lot of discussions about everything and physics.

I am grateful to the Italians for swimming excursions and "Aperos" and to Sarah for lunch in H2 once a week (not only!).

And last but not least I want to thank my family and Pierre-Jean, who always supported me.

Ich versichere, dass ich diese Arbeit selbständig verfasst und keine anderen als die angegeben Quellen und Hilfsmittel benutzt habe.

Heidelberg, den 03.06.2007 .....

(Unterschrift)